

Magnetization reversal
processes in stripes with
perpendicular magnetic
anisotropy

Maciej Urbaniak
Instytut Fizyki Molekularnej
Polskiej Akademii Nauk

Poznań, 2014.11.14

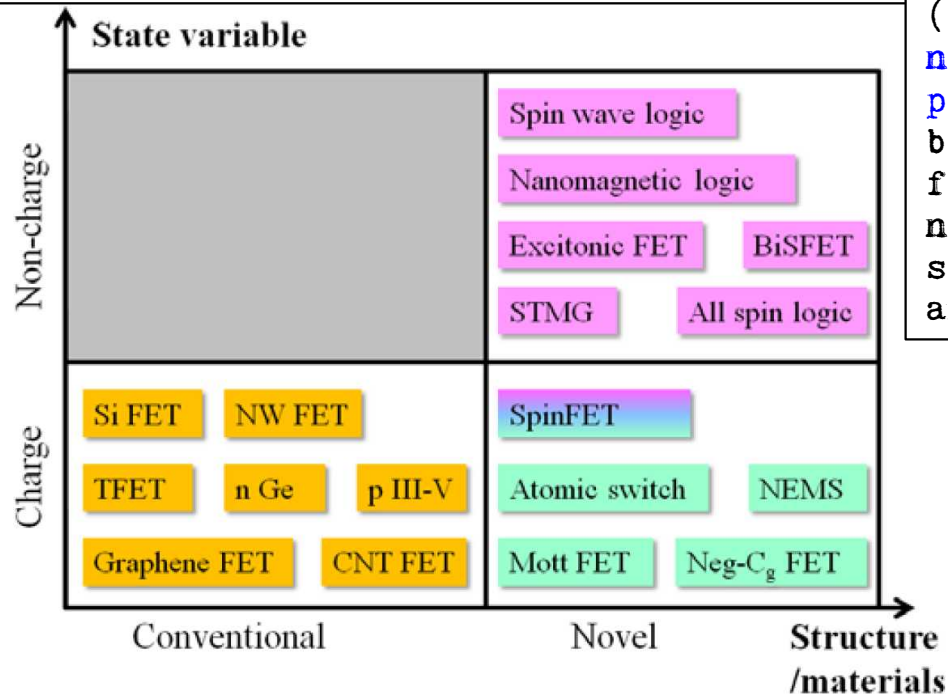
Outline

- 1 Magnetization reversal in perpendicular magnetic anisotropy systems
- 2 Systems with switching field gradients
- 3 Preparation and bombardment of Co/Au patterned films
- 4 Magnetization reversal in Co/Au stripes with graded effective anisotropy
- 5 Conclusions

New applications of perpendicular anisotropy materials

Nanomagnetic logic (NML) [1,6]:

- Magnets with PMA possess a bistable out of plane magnetization state, which is encoded with the Boolean logic states "1" and "0"
- Neighboring magnets interact by field-coupling enabling the realization of signal transmitting inverter chains
- NML implementation are capable of retaining state without power and could be radiation hard.



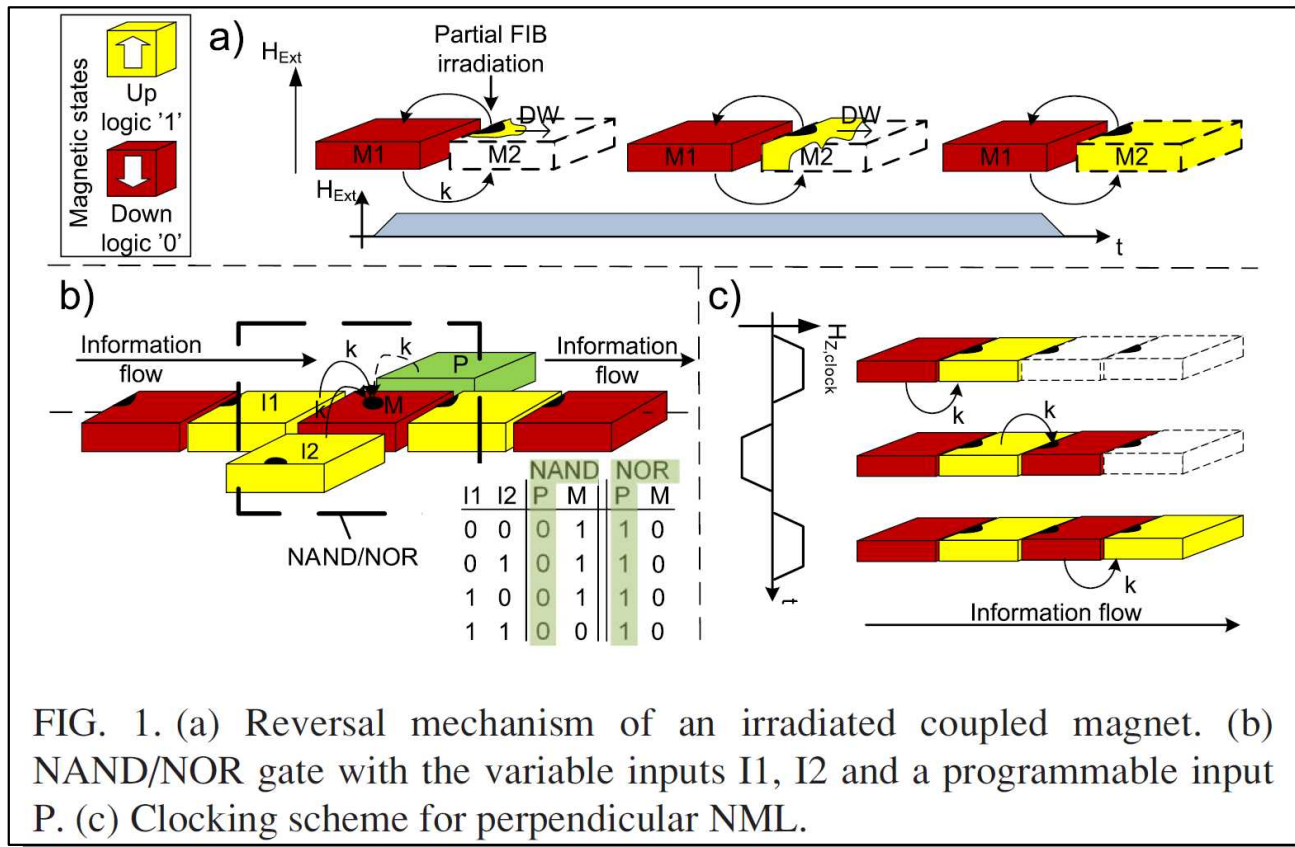
"Perpendicular magnetic logic (PML) devices **switch through nucleation and domain wall propagation**. This reversal behavior is markedly different from in-plane permalloy nanomagnets, which remain nearly single-domain during switching and rotate coherently." [6]

Figure ERD5 Taxonomy of options for emerging logic devices. The devices examined in this chapter are differentiated according to (1) whether the structure and/or materials are conventional or novel, and (2) whether the information carrier is electron charge or some non-charge entity. Since a conventional FET structure and material imply a charge-based device, this classification results in a three-part taxonomy.

New applications of perpendicular anisotropy materials

Nanomagnetic logic (NML) [1]:

- Magnets with PMA possess a bistable out of plane magnetization state, which is encoded with the Boolean logic states "1" and "0"
- Neighboring magnets interact by field-coupling enabling the realization of signal transmitting inverter chains
- Directed signal flow in perpendicular NML is provided by partial **focused ion beam (FIB)** irradiation



Superposition of external field and field from neighbor cell reverses a given cell

New applications of perpendicular anisotropy materials

Nanomagnetic logic (NML) [1]:

- Magnets with PMA possess a bistable out of plane magnetization state, which is encoded with the Boolean logic states "1" and "0"
- Neighboring magnets interact by field-coupling enabling the realization of signal transmitting inverter chains
- Directed signal flow in perpendicular NML is provided by partial **focused ion beam (FIB) irradiation**

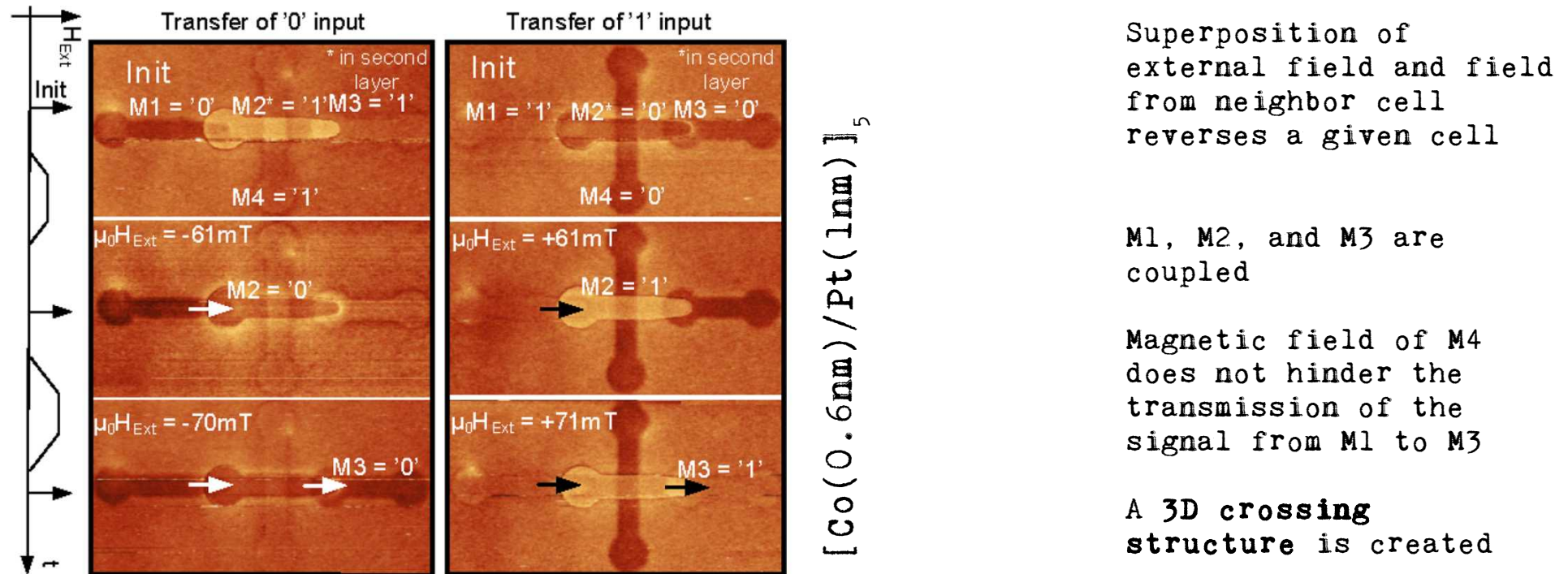
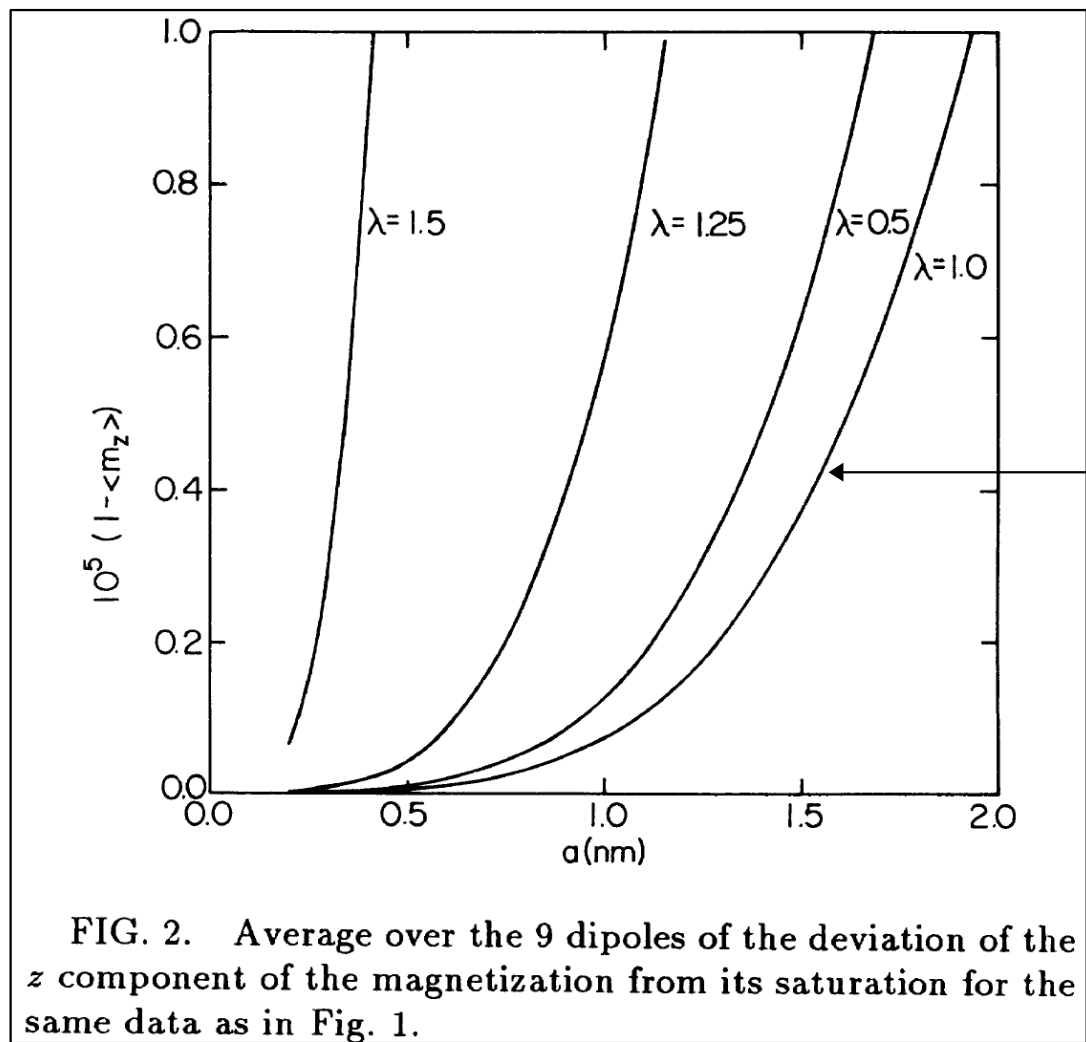
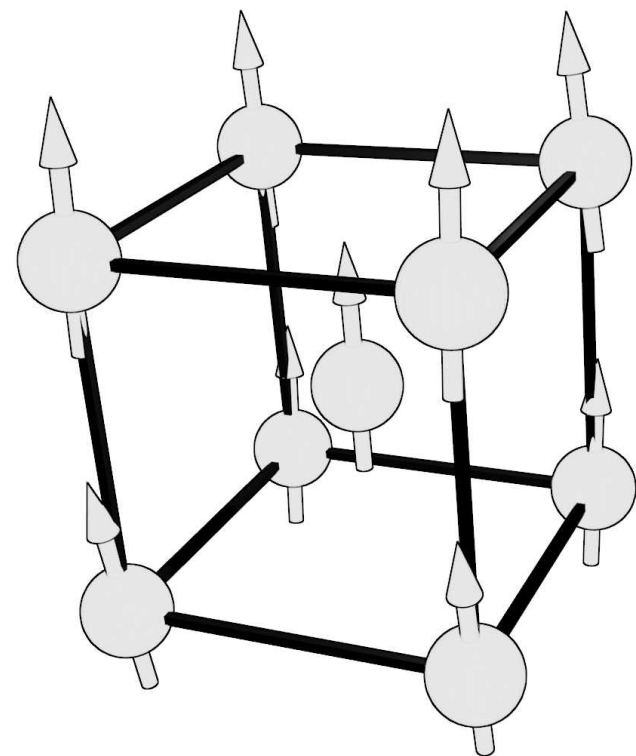


FIG. 5. MFM measurements of directed signal flow. The magnetization state of M1 is first transferred to M2 and then from M2 to M3 proving directed signal flow from left to right.

Nucleation centers



$\lambda=1$ - bcc



$$E = E_{exchange} + E_{aniotropy} + E_{dipolar}$$

$(\pm 1, \pm 1, \pm 1), (0, 0, 0)$ - positions of spins

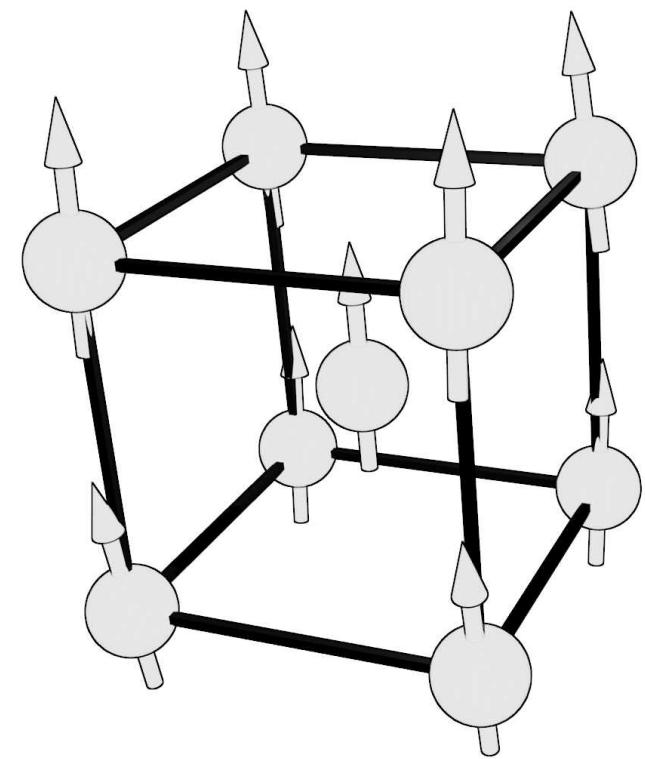
$-\lambda(1, 1, 1)$ - position of the 9th spin

>> For somewhat larger, but rather small particles there is no "critical" size below which a particle is uniformly magnetized. <<

Nucleation centers

*"The concept of a **nucleation field** as the field at which the magnetization just start to deviate from saturation, cannot be defined as rigorously as assumed before, now that it has been shown that the saturated state cannot exist.*

However, the obtained deviations from uniformity are extremely small, and their contribution can be ignored, whenever common sense indicates that very small deviations can only have a small effect." - A. Aharoni



$$E = E_{\text{exchange}} + E_{\text{anisotropy}} + E_{\text{dipolar}}$$

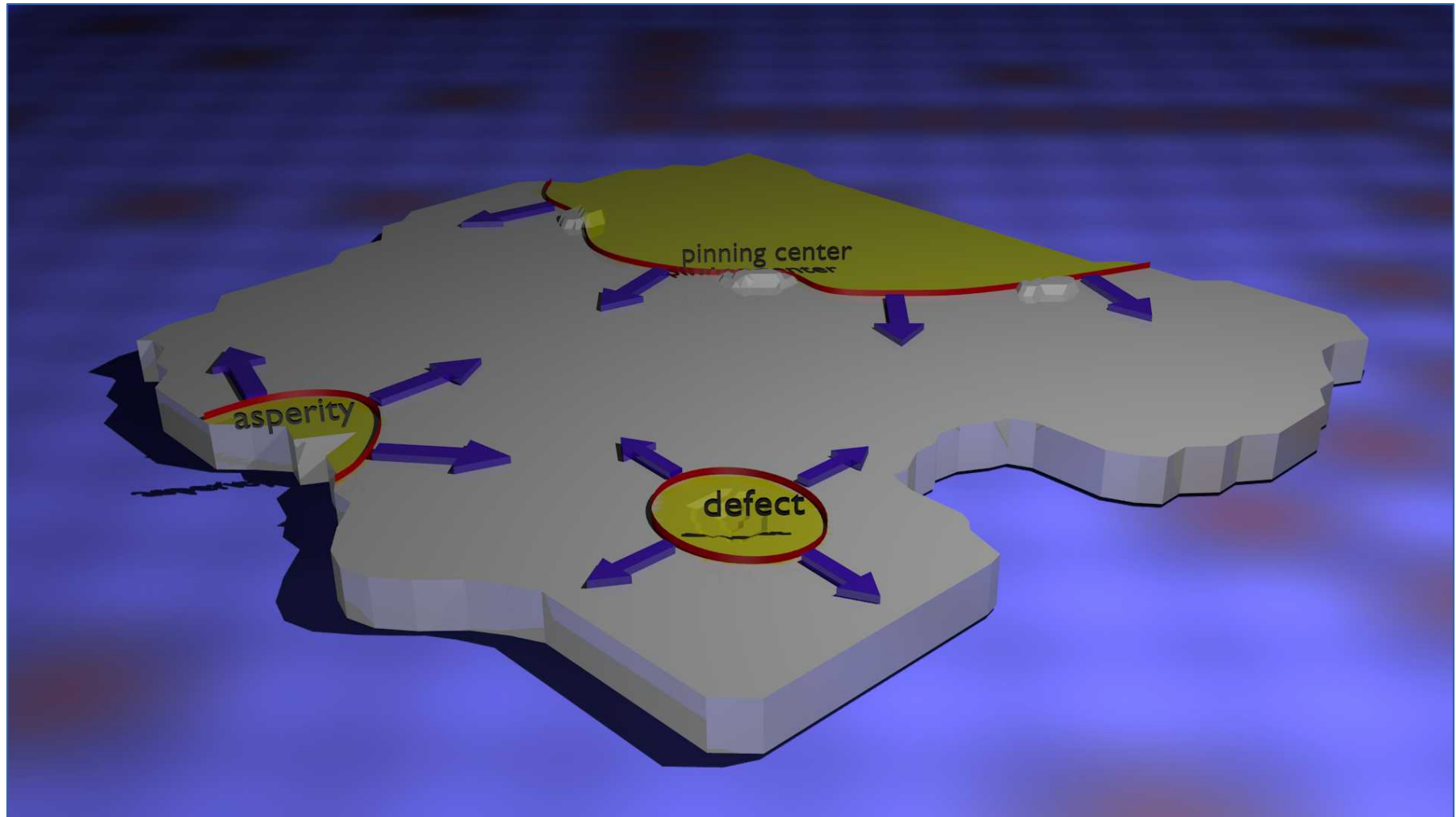
$(\pm 1, \pm 1, \pm 1), (0, 0, 0)$ - positions of spins

$-\lambda(1, 1, 1)$ - position of the 9th spin

>>For somewhat larger, but rather small particles there is no "critical" size below which a particle is uniformly magnetized.<<

Domain walls and hysteresis

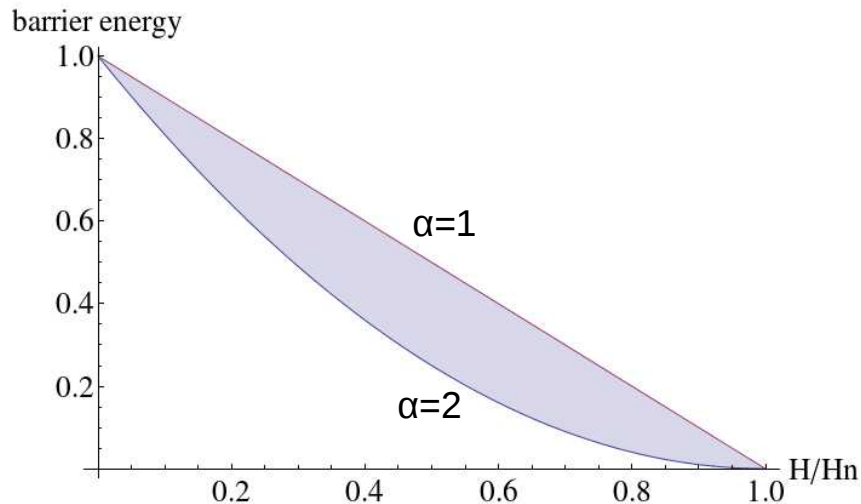
- The wall can nucleate at defect, thermal fluctuation, surface asperity (change of anisotropy or exchange constant)
- The movement of wall can be hindered by pinning centers



Nucleation in thin films

- The barrier height to nucleation (phenomenology):

$$\Delta E = E_n \left(1 - \frac{H}{H_n}\right)^\alpha \quad 1 \leq \alpha \leq 2, \quad E_n, H_n - \text{nucleation energy and field}$$



- **Coherent rotation inside the nucleation volume** (V_n) - like in Stoner-Wohlfarth model of small particles the E_n is equal to the product of anisotropy and V_n .
- Nucleation volume and nucleation field are very sensitive to the local environment, but in thin films with large grains one can approximate [3]:

$$V_n \approx \delta_w \cdot t, \quad \delta_w - \text{DW width, } t - \text{film thickness}$$

- In our Co/Au MLs V_n from the above formula is approx. 400 nm^3 .

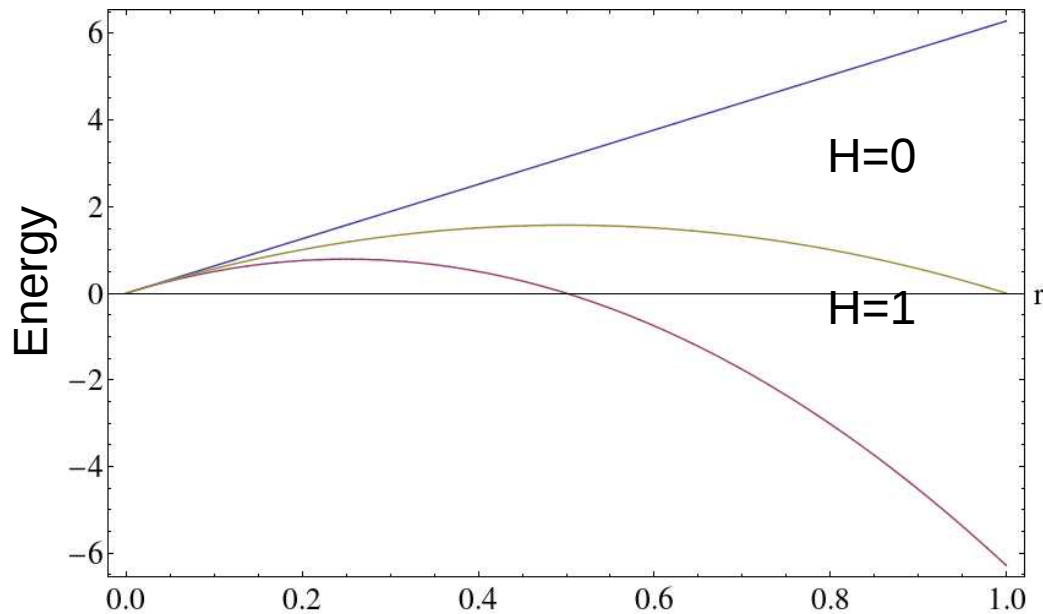
Nucleation in thin films

The droplet model:

-the energy of the inverse bubble is composed of Zeeman energy and domain wall energy:

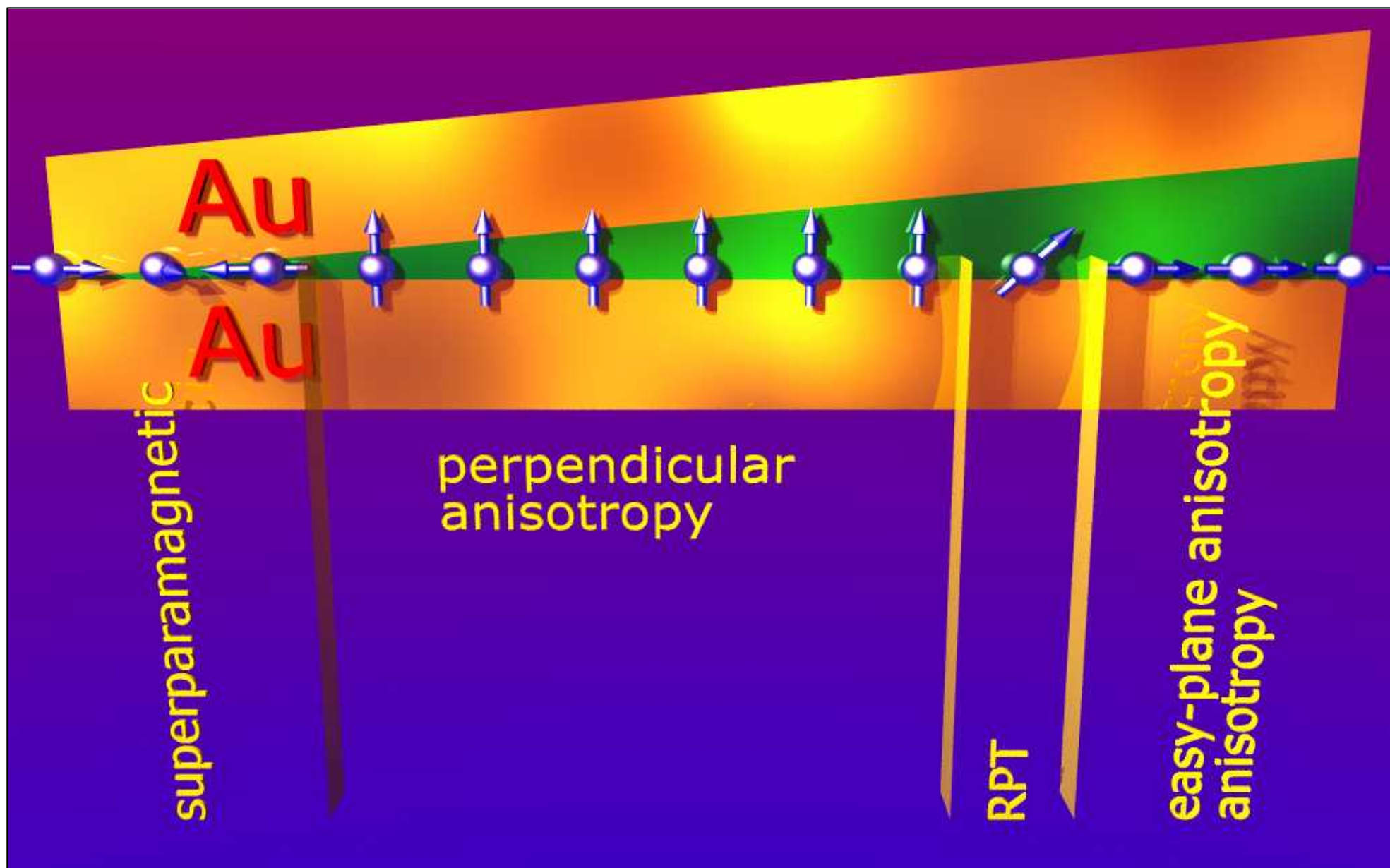
$$E(r) = 2\pi r \gamma t - 2\pi r^2 t \mu_0 H M_s,$$

γ -DW energy per unit area

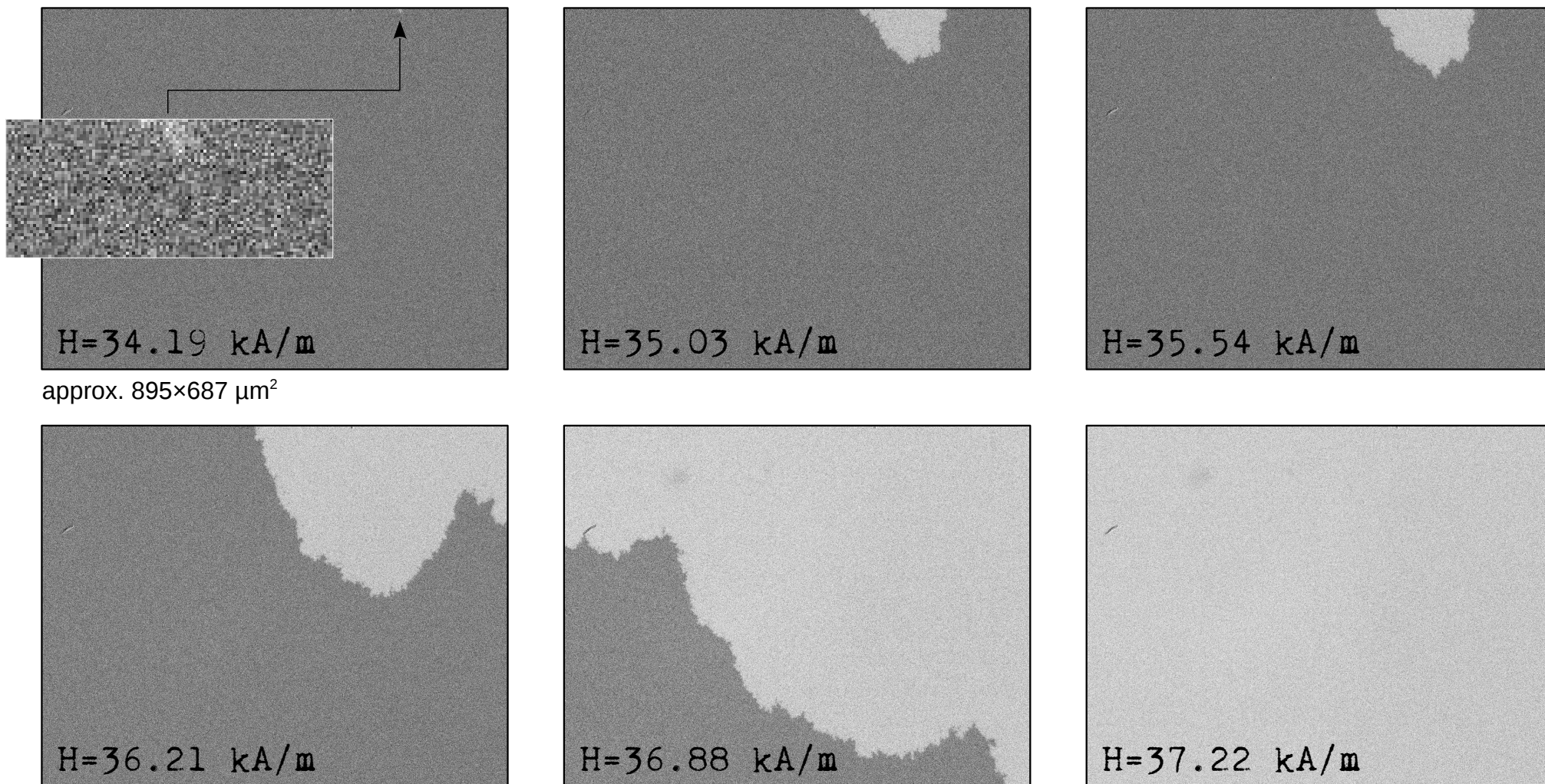


- If the reversed domain reaches the critical radius its energy decreases as it grows
- Energy barrier is infinite for H=0
- The model was used for Co/Pt thin films

Perpendicular anisotropy in Co/Au, Co/Pt etc. MLs

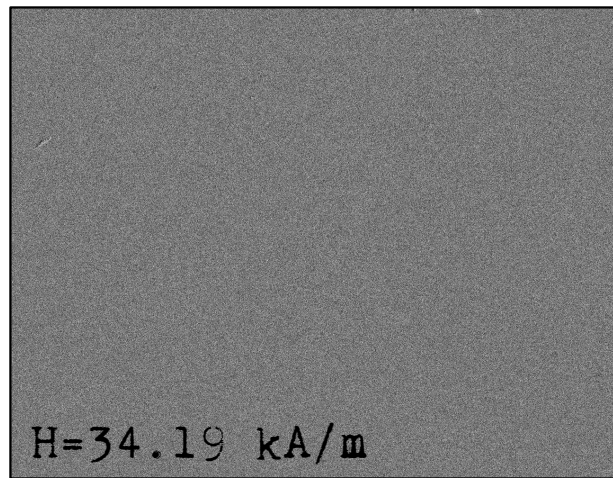


Domain wall propagation driven reversal in $(\text{Co}/\text{Au})_2$ films

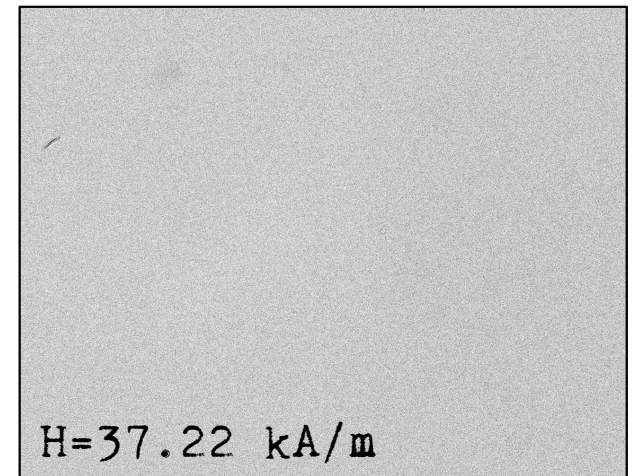
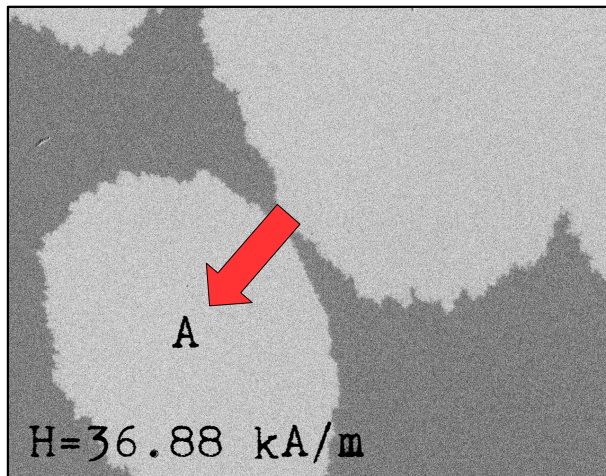
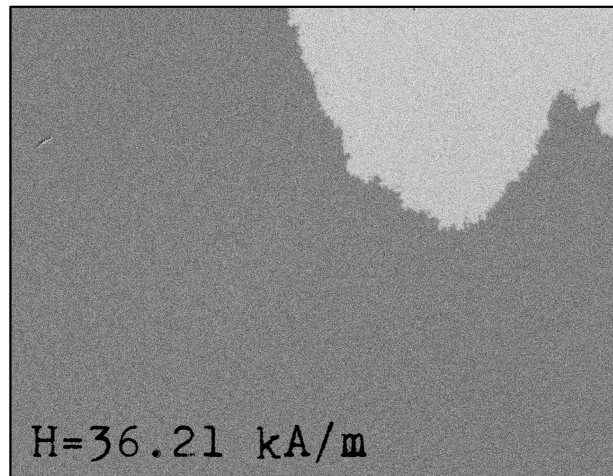
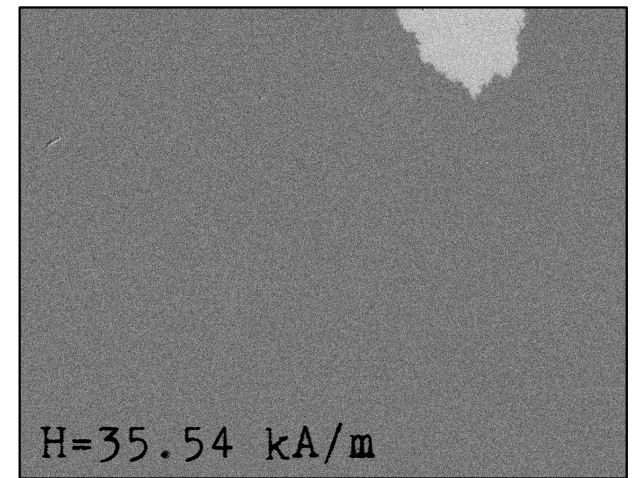
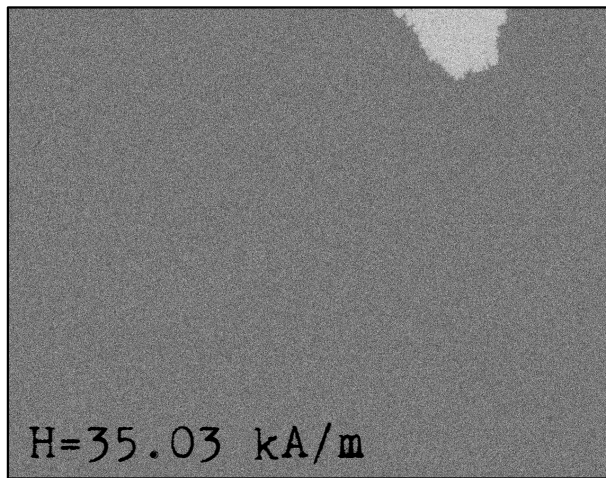


In good quality films deposited by sputtering the density of nucleation centers can be very low. For the series of images shown above there seems to be no nucleation center within the image (approx. $1 \times 0.8 \text{ mm}^2$)

Domain wall propagation driven reversal in $(\text{Co}/\text{Au})_2$ films



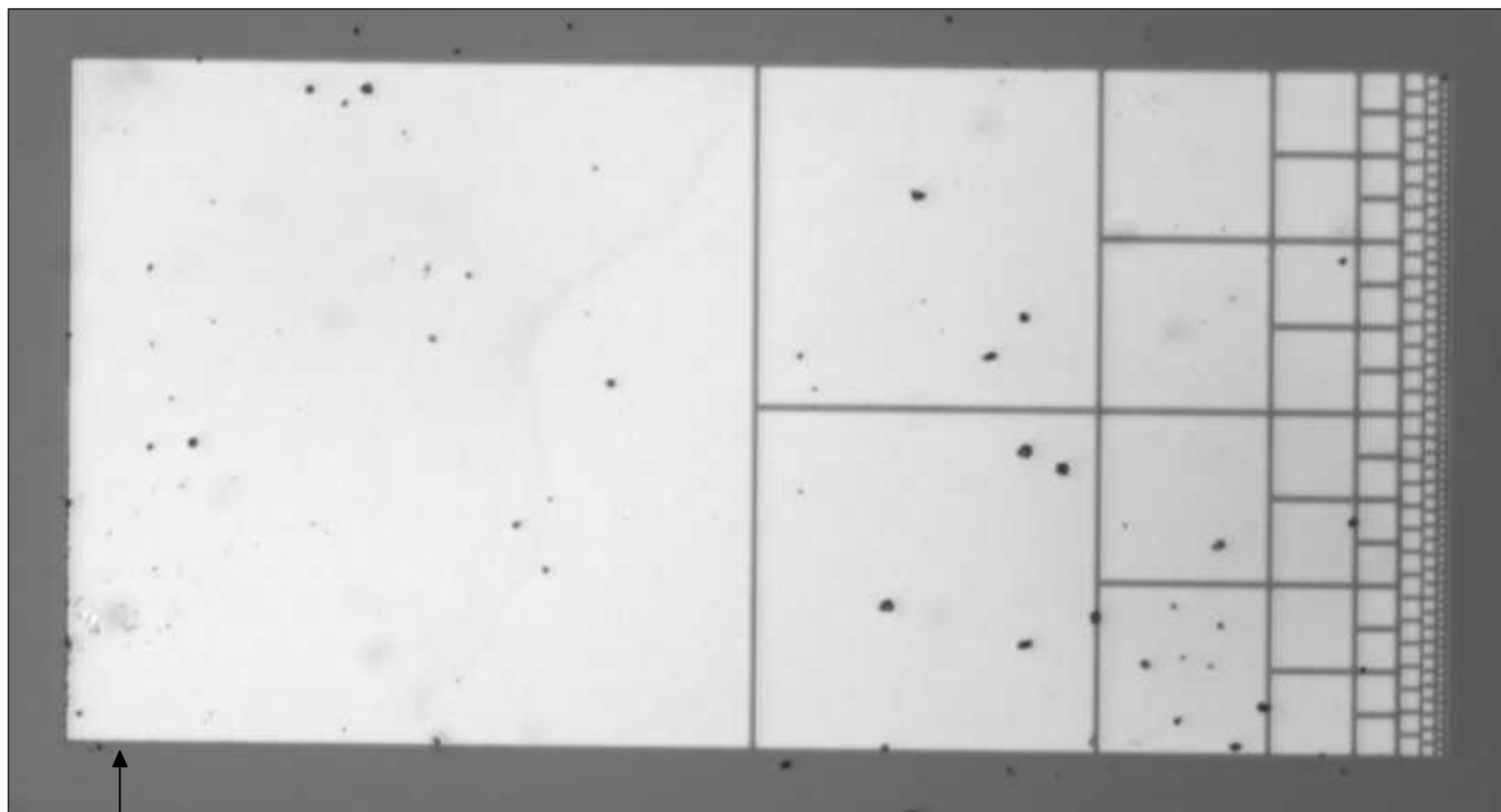
approx. $895 \times 687 \mu\text{m}^2$



The exact evolution of the domains is not reproducible as evidenced by a domain expanding from the probable nucleation center near the point A.

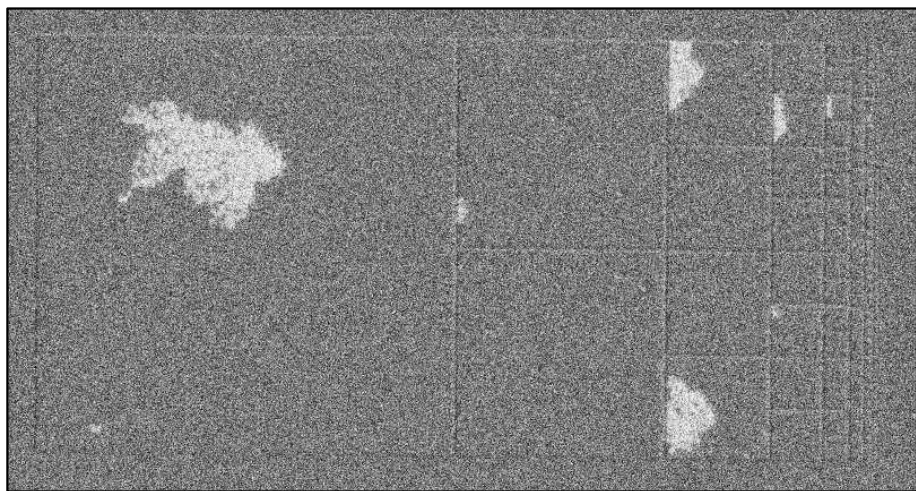
Domain wall propagation driven reversal in $(\text{Co}/\text{Au})_2$ films

Patterned structure of the type used for the investigation of nucleation centers density (optical microscopy image):

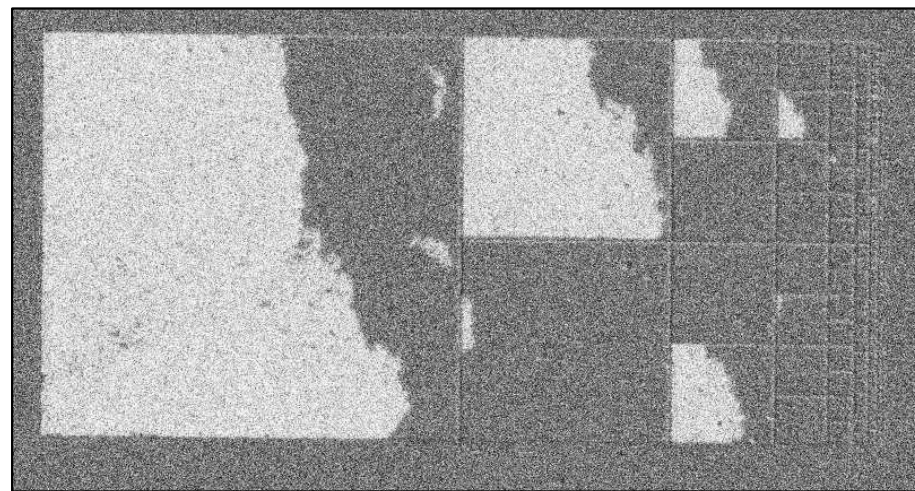


256 x 256 μm

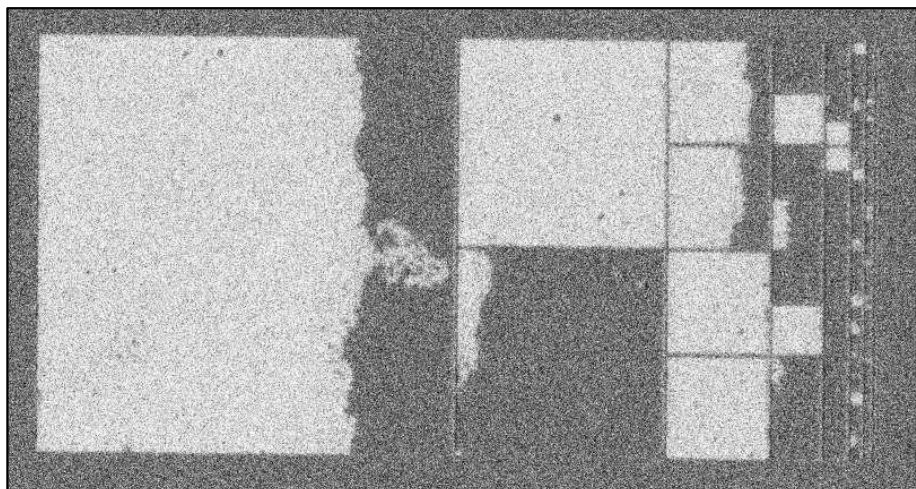
Domain wall propagation driven reversal in $(\text{Co}/\text{Au})_2$ films



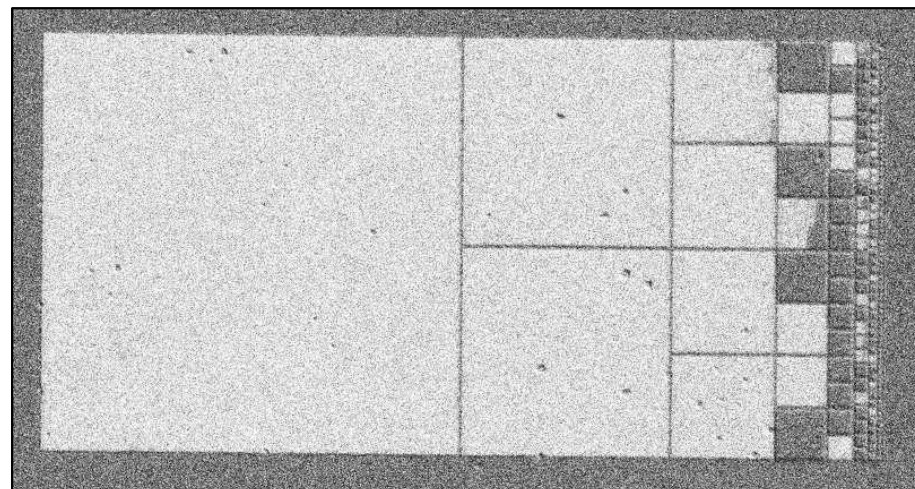
H=34.7 kA/m



H=36.38 kA/m



H=37.22 kA/m



H=37.89 kA/m

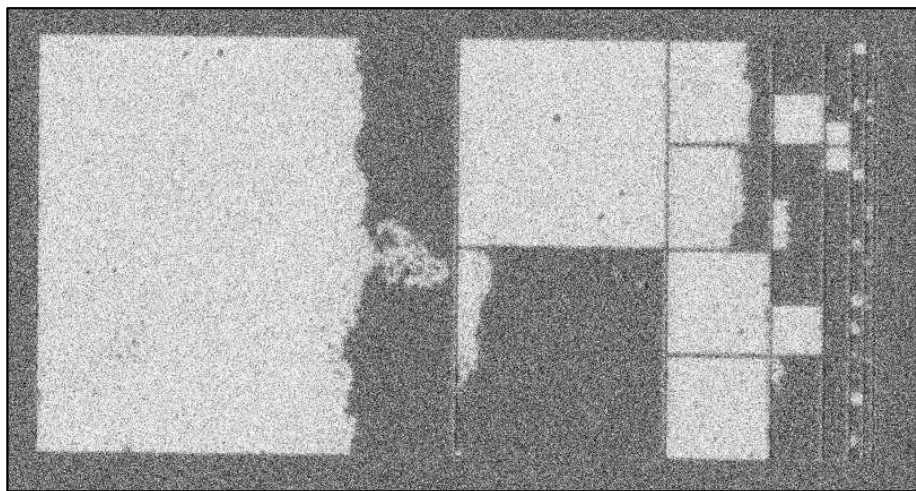
In high quality layers the reversal depends strongly on the element size (assuming the elements do not interact).

Kerr microscopy images

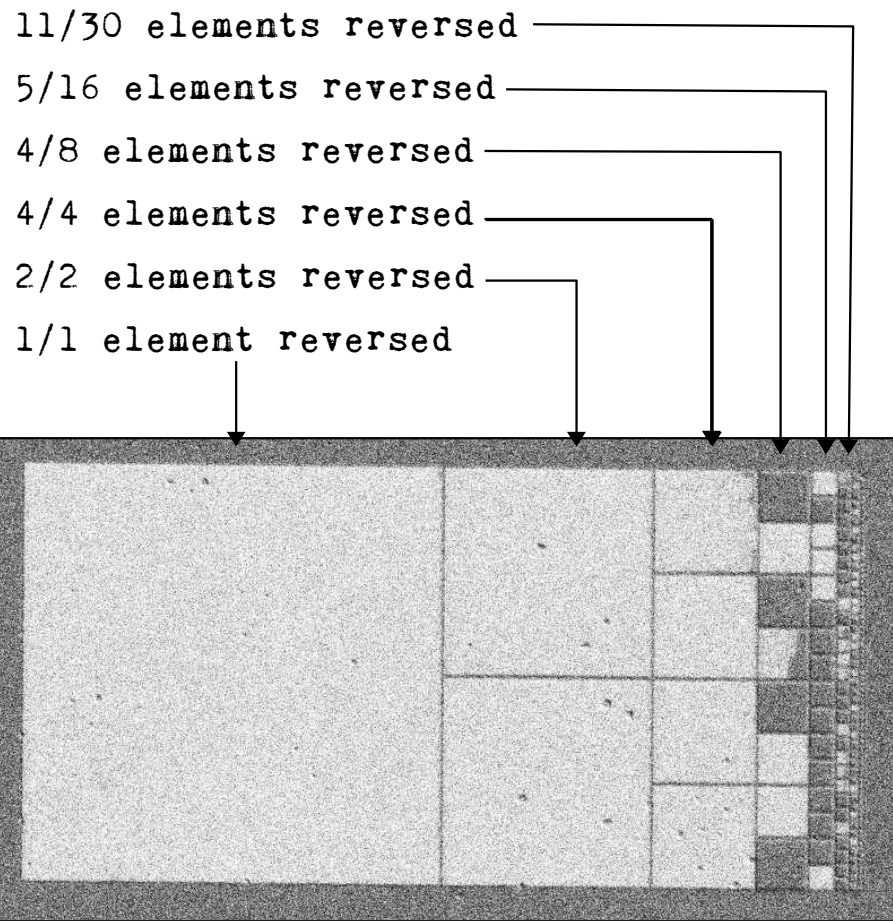
Domain wall propagation driven reversal in $(\text{Co}/\text{Au})_2$ films

The probability of activating the nucleation center is roughly proportional to element area.

If nucleation centers areal density is low the large elements may reverse while the small ones do not.



H=37.22 kA/m



H=37.89 kA/m

In high quality layers the reversal depends strongly on the element size (assuming the elements do not interact).

Tailoring nucleation fields in perpendicular anisotropy wires

- Pt(5nm)/[Co(0.7nm)/Au(2nm)]₄ on silicon nitride membrane, electron-beam lithography, sputtering, lift-off processing
- Magnetic contrast is based on the x-ray magnetic circular dichroism (XMCD) effect. It is proportional to the magnetization components along the projection of the x-ray beam. The perpendicularly magnetized sample was inserted into the microscope setup such that the surface normal was in parallel to the beam direction.

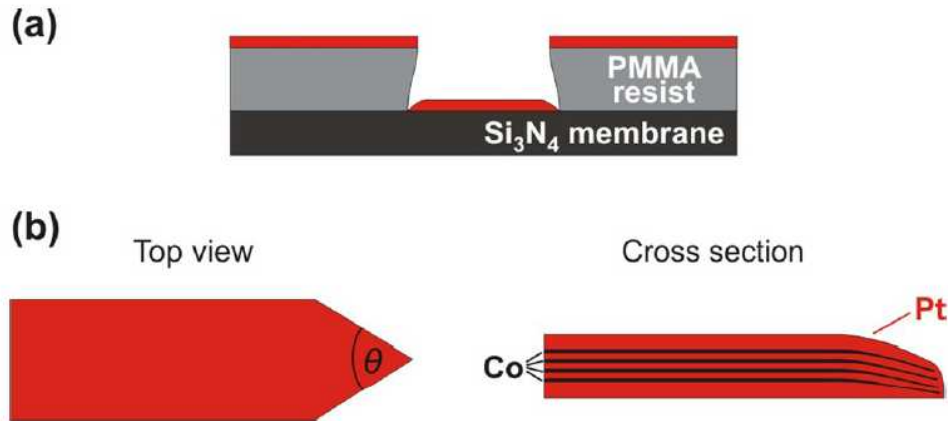


FIG. 1. (a) Illustration of sample preparation. (b) Wire geometry: due to shadowing by the resist mask during sputter deposition of the metal film, less material is deposited at the triangular-pointed wire end with tip-opening angle θ .

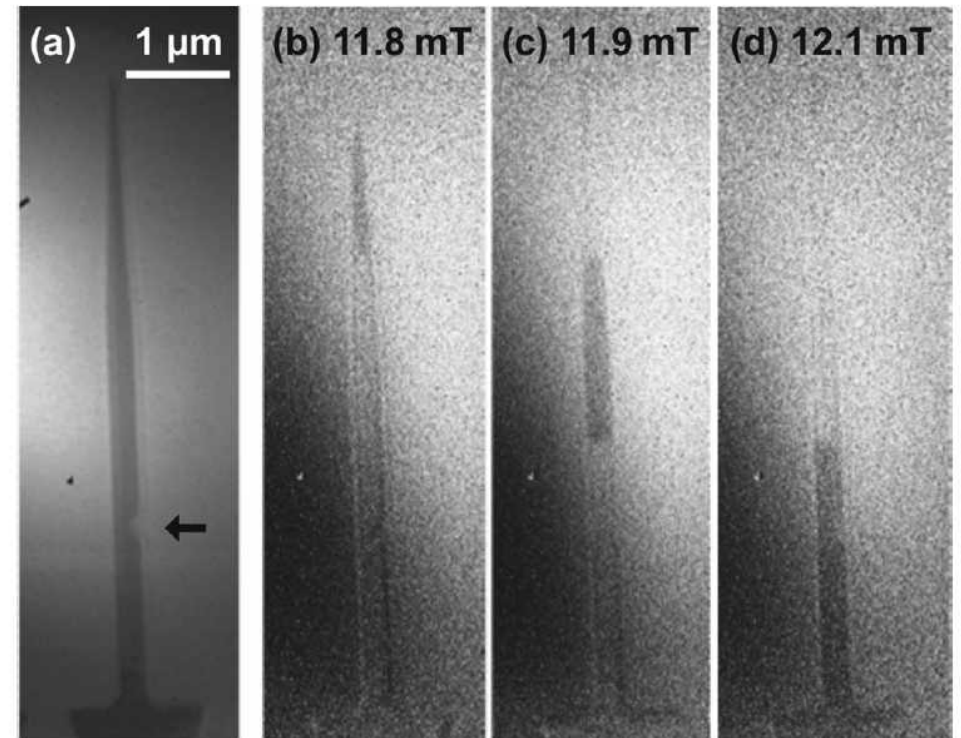


FIG. 2. (a) Transmission x-ray micrograph and (b) through (d) corresponding differential images (the respective previous image serves as reference) of a Pt(5.0nm)/[Co(0.7nm)/Pt(2.0nm)]₄ wire with a nucleation pad (bottom, not completely visible), a notch marked by the arrow in (a), and a triangular-pointed end (top) recorded at the given field values after saturation at -200 mT.

Tailoring nucleation fields in perpendicular anisotropy wires

- Pt(5nm)/[Co(0.7nm)/Au(2nm)]₄ on silicon nitride membrane, electron-beam lithography, sputtering, lift-off processing

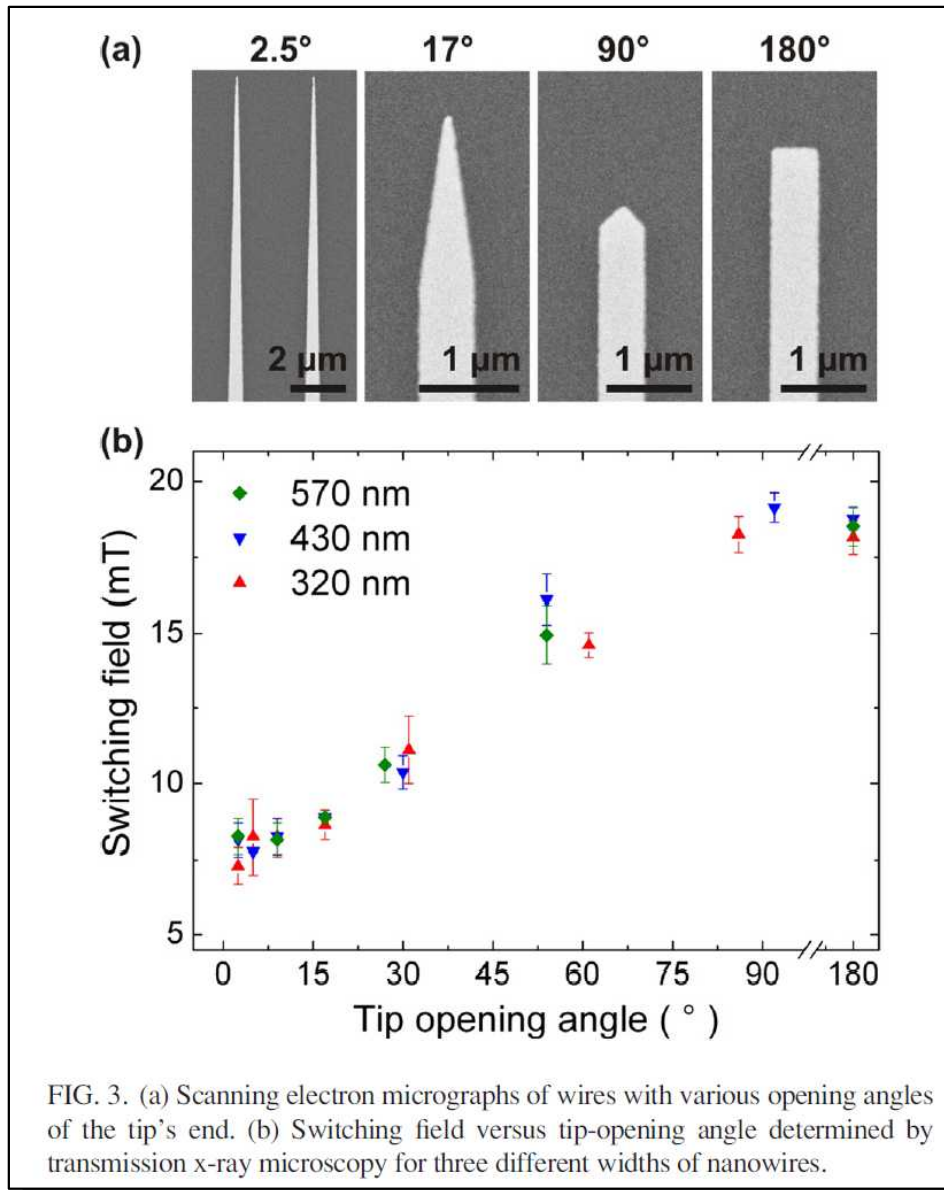
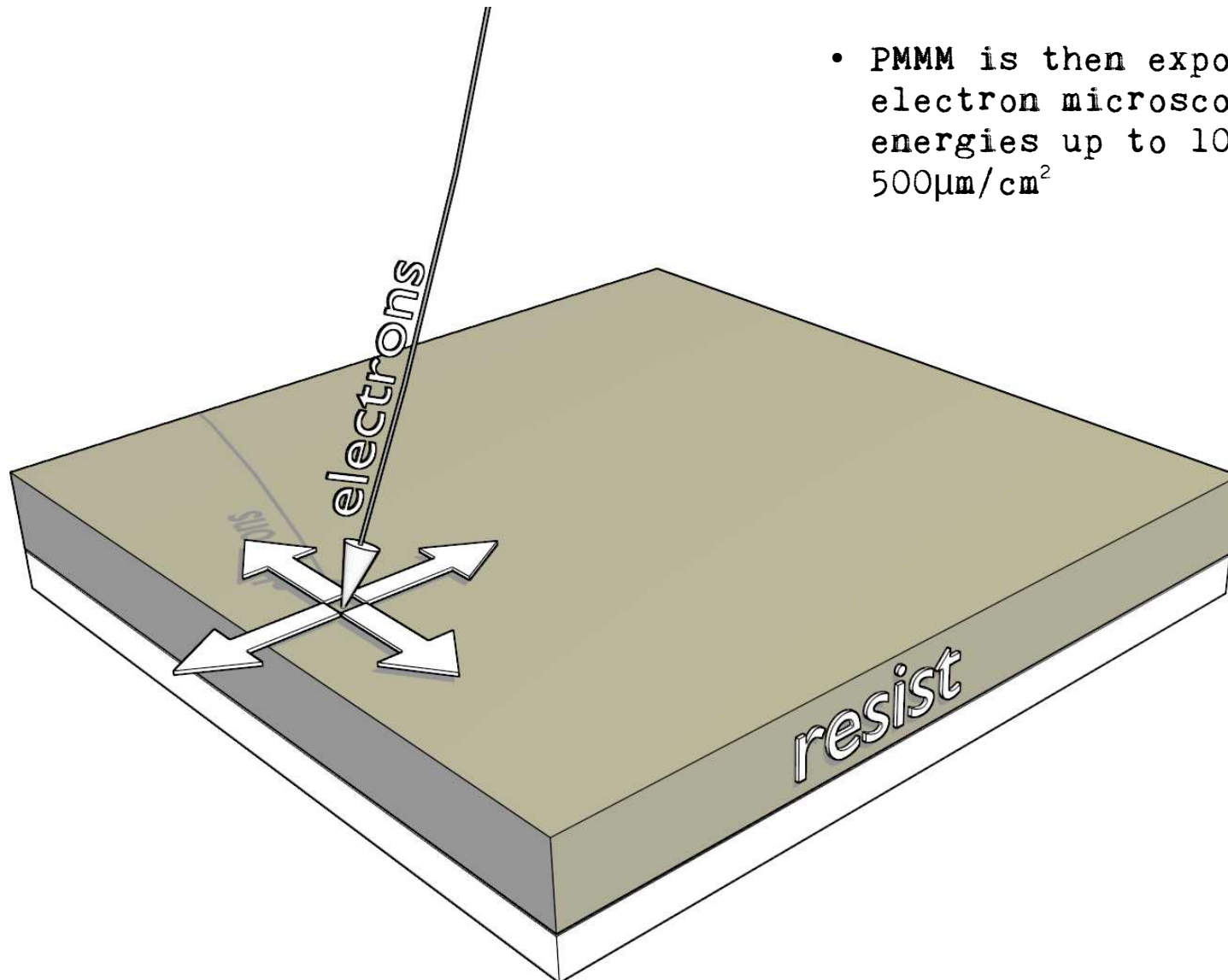


FIG. 3. (a) Scanning electron micrographs of wires with various opening angles of the tip's end. (b) Switching field versus tip-opening angle determined by transmission x-ray microscopy for three different widths of nanowires.

- "We have shown that the critical field for the nucleation and injection of domain walls in Co/Pt nanowires can be **tuned and reduced by up to about 60%** compared to the switching field of rectangular-shaped wires by designing triangularly pointed wire ends." [5]
- In in-plane anisotropy layers the triangular-pointed ends increase the nucleation field
- The nucleation field decrease in PMA MLs is a consequence of:
 - decreased PMA due to shadowing effects
 - increased of nucleation area in sharper tips

Sample preparation

- Si(100) substrate is covered with roughly 350nm of PMMA* [Poly(methyl 2-methylpropenoate), $(C_5O_2H_8)_n$] using spin coater at 4000 rpm.
- PMMA is baked at approx. 170°C on a hot-plate

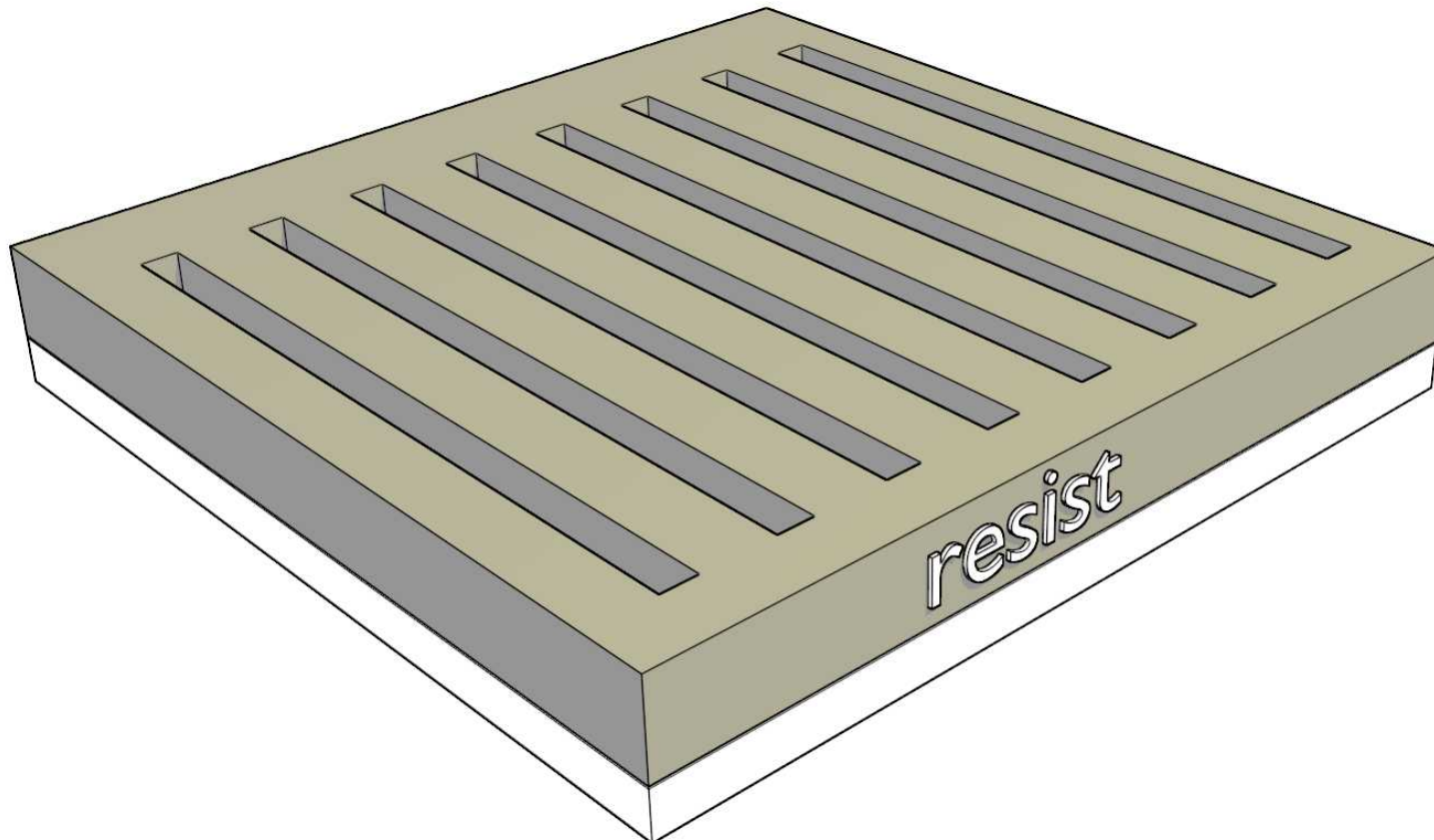


- PMMM is then exposed with a scanning electron microscope with electron energies up to 10keV and doses up to $500\mu\text{m}/\text{cm}^2$

*known, among others, as Plexiglas

Sample preparation

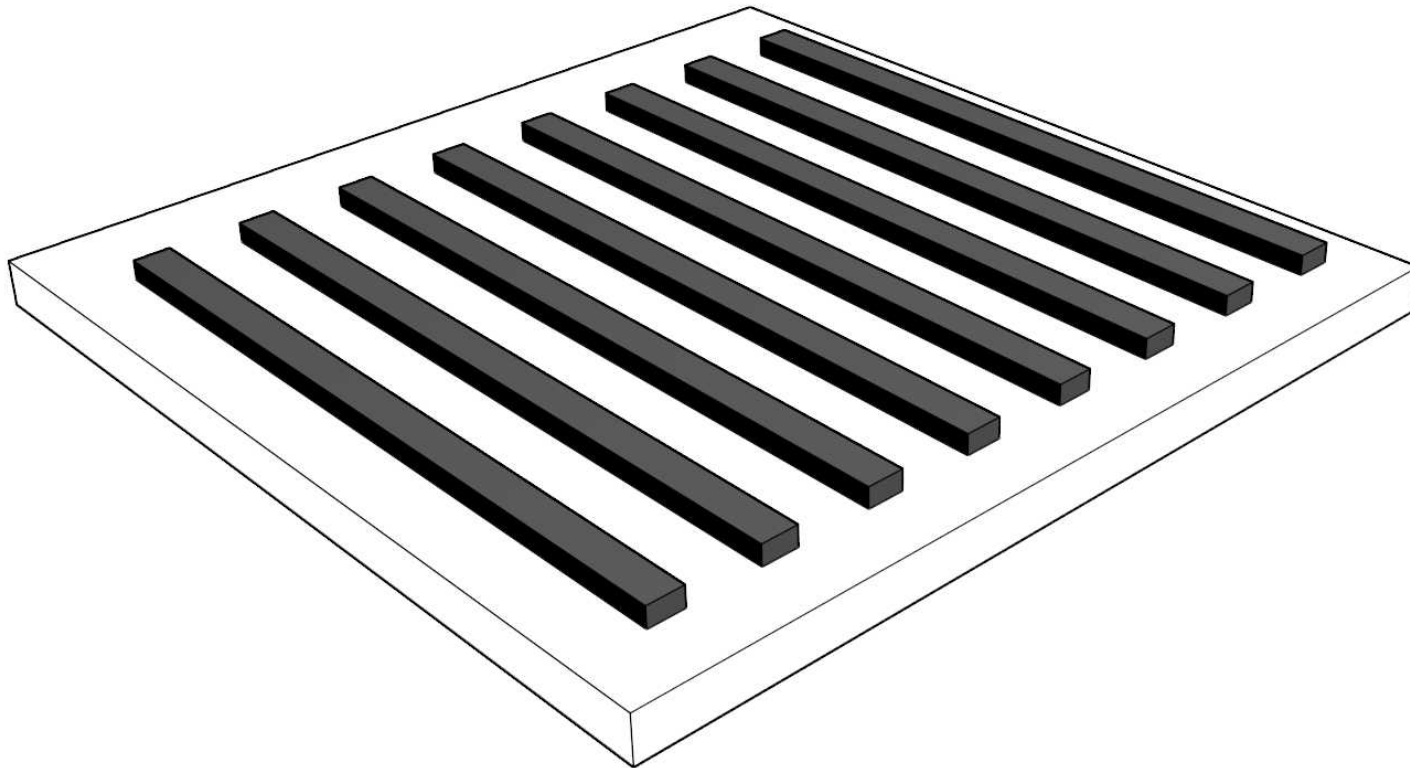
- Si(100) substrate is covered with roughly 350nm of PMMA* [Poly(methyl 2-methylpropenoate), $(C_5O_2H_8)_n$] using spin coater at 4000 rpm.
- PMMA is baked at approx. 170°C on a hot-plate
- ...and then developed with methyl isobutyl ketone (MIBK)
- the developed PMMA is rinsed out leaving the mask for the sputtering



*known, among others, as Plexiglas

Sample preparation

- Ti(4nm)/Au(60nm)/[Co(0.8nm)/Au(1nm)]₂ MLs are sputtered on the lithography mask
- Lithography mask and the excess MLs rinsed out
- The distance between the neighboring stripes ensures weak interaction between them (domain walls do not influence each other) - spatial period about 0.11mm
- Length - 990μm, widths from 2 to 20μm.



Perpendicular anisotropy in Co/Au, Co/Pt etc. MLs - influence of ion bombardment

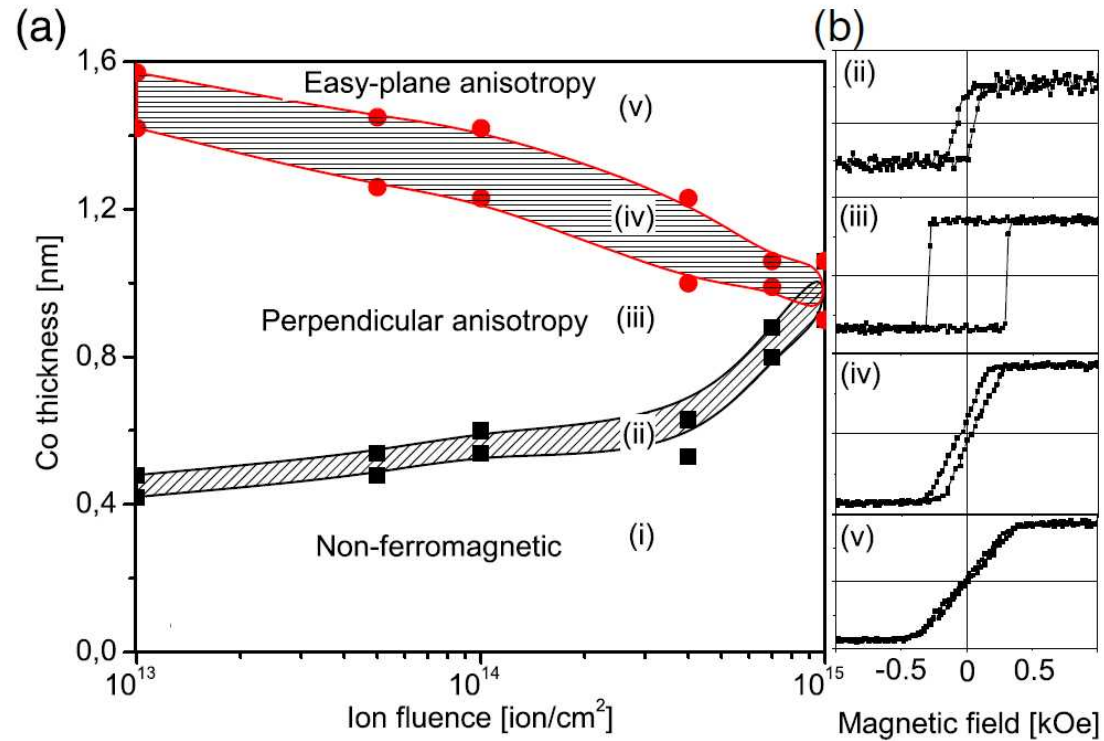
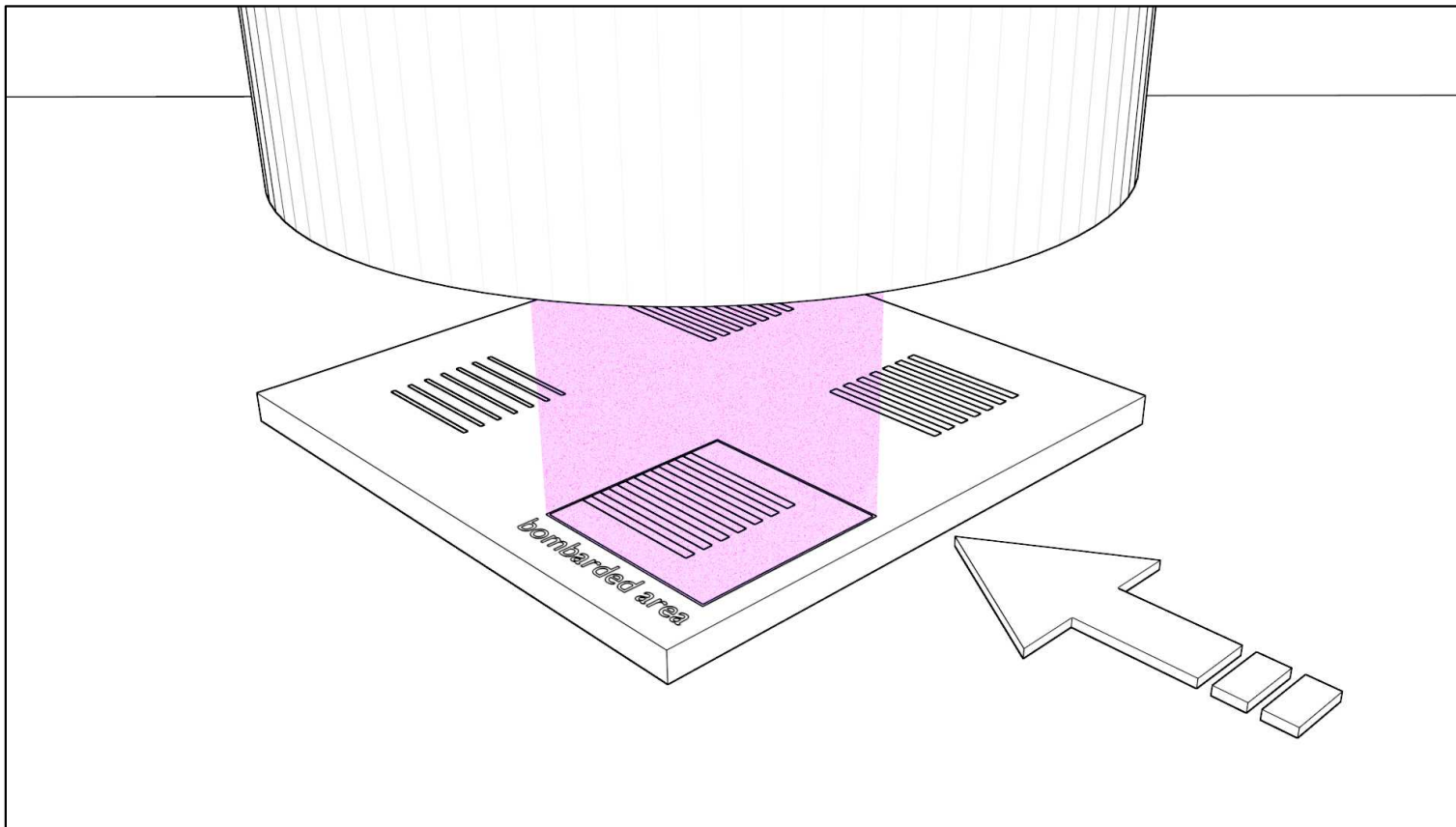


Figure 3. Magnetic phase changes of the Co layer as a function of Co layer thickness caused by bombardment with 10 keV He⁺ ions. (a) Variation of the Co thickness intervals (i)–(v) as a function of He⁺ ion fluence. (b) Hysteresis loops corresponding to thickness intervals (ii)–(v). Dashed areas (ii) and (iv) are guides to the eye for the transition regimes.

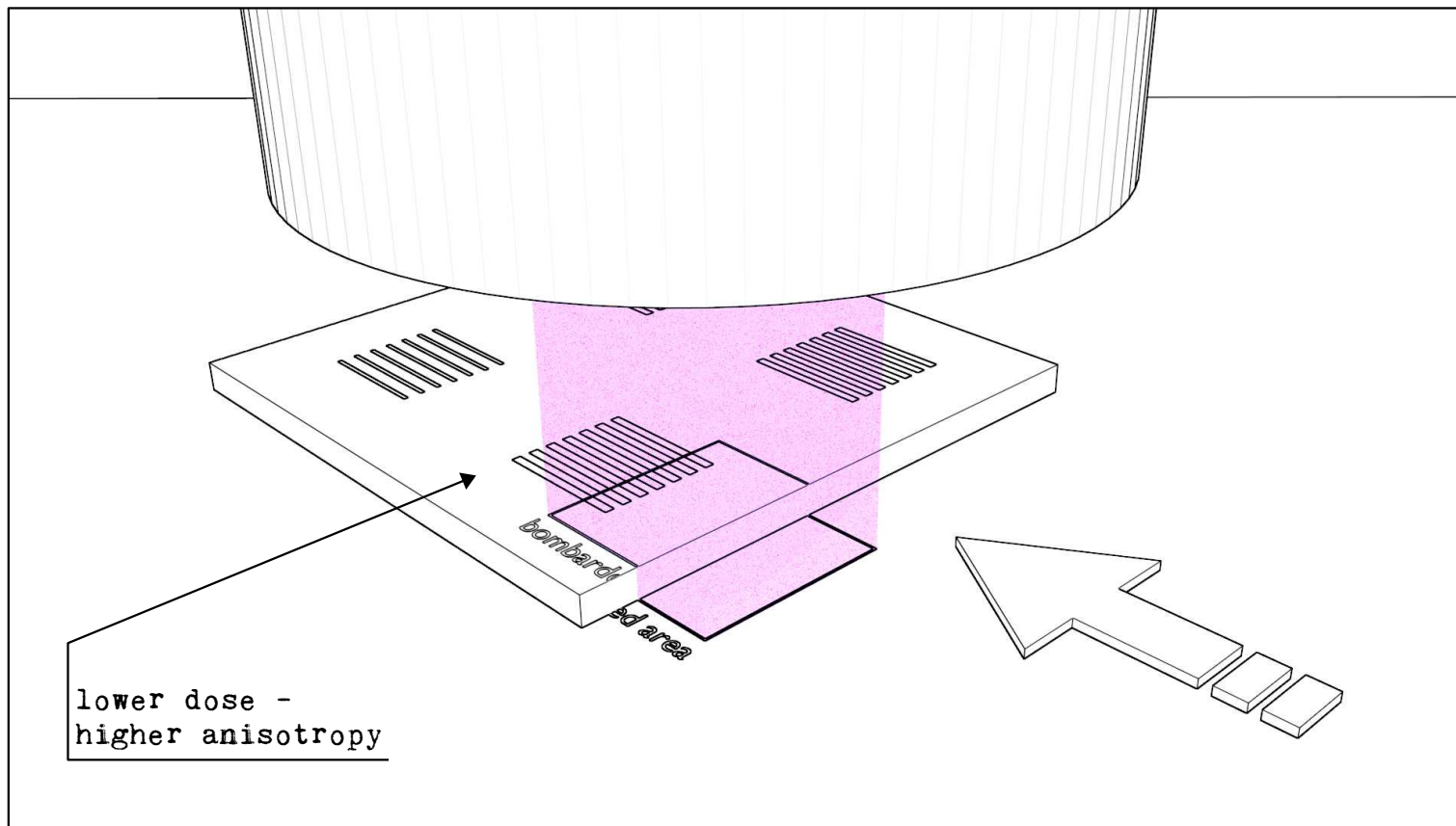
Ion bombardment of the stripes

- Sample holder moves along the longer edges of the stripes and ion dose gradient is created along the stripes
- He⁺ ion doses are up to 10¹⁵ ion/cm²
- The dose changes linearly from approx. 0 to 10¹⁵ ion/cm² over the length of the stripes (990μm)
- The 10¹⁵ ion/cm² dose corresponds to approx. **one He⁺ ion for seven Co atoms**



Ion bombardment of the stripes

- Sample holder moves along the longer edges of the stripes and ion dose gradient is created along the stripes
- He⁺ ion doses are up to 10^{15} ion/cm²
- The dose changes linearly from approx. 0 to 10^{15} ion/cm² over the length of the stripes (990 μ m)
- The 10^{15} ion/cm² dose corresponds to approx. **one He⁺ ion for seven Co atoms**



Ion bombardment of the extended samples

- Ion dose gradient results in coercive field gradient

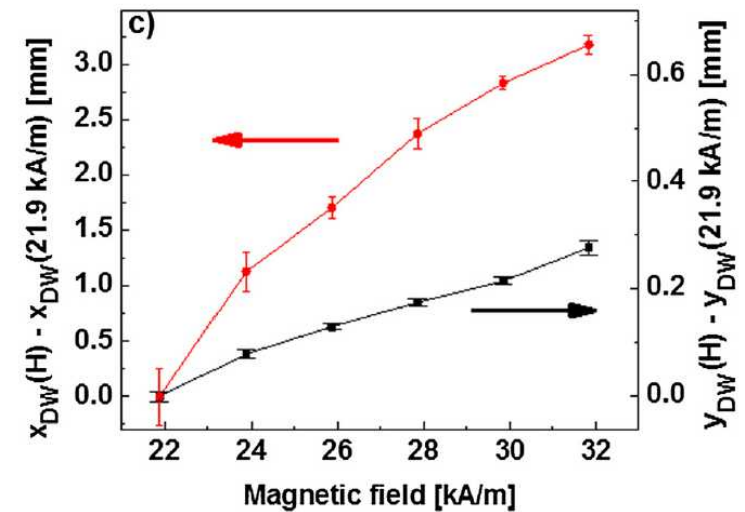
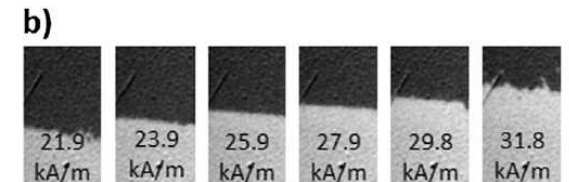
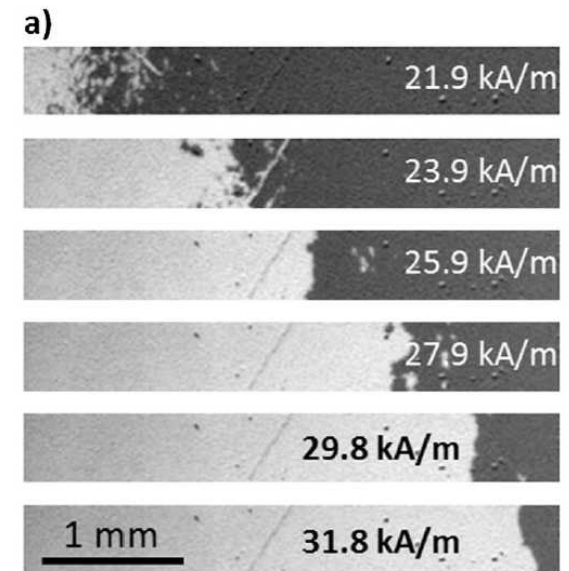
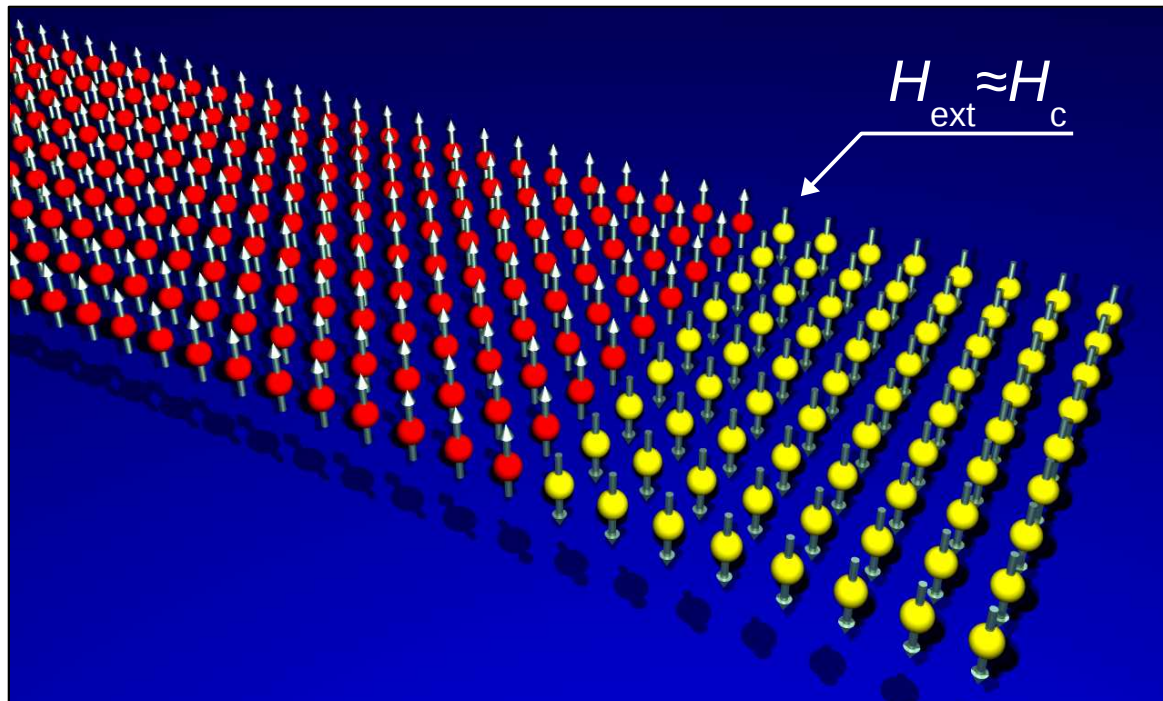
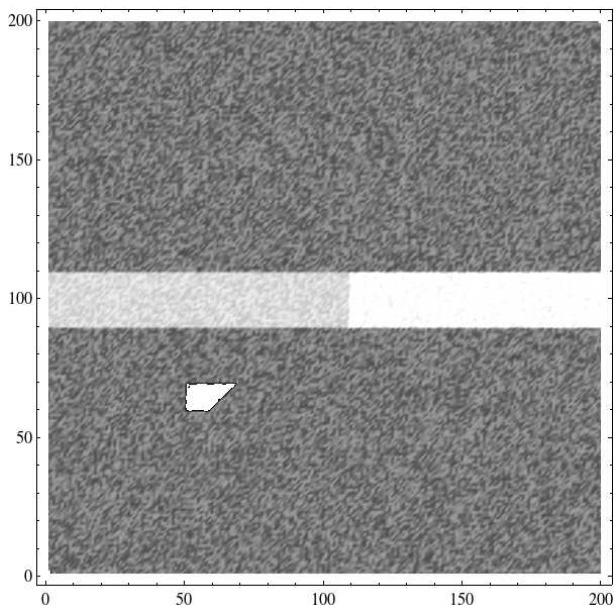
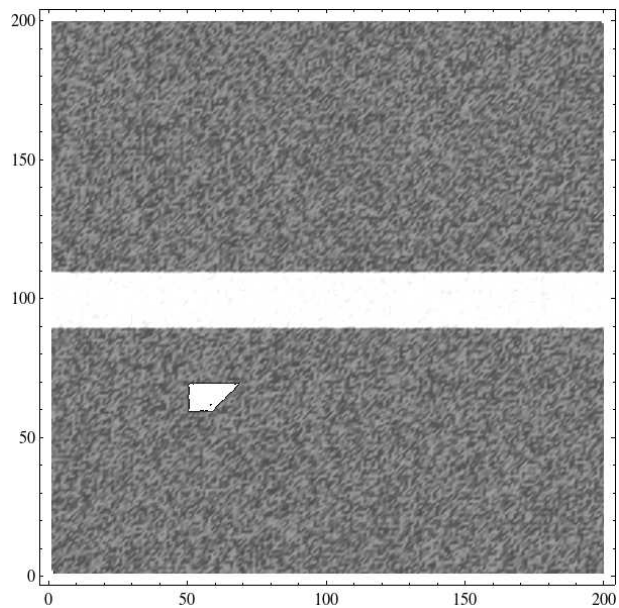
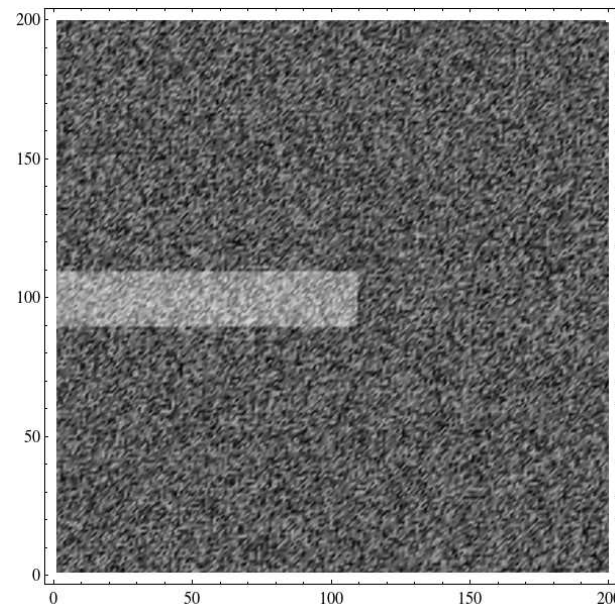


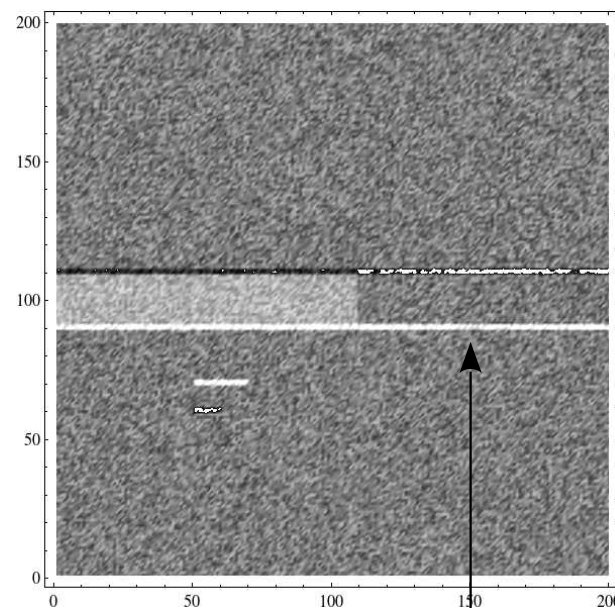
Figure 3 Domain wall propagation for two different coercive field gradients. Propagation of the DW in the region with small (a) and high (b) coercive field gradient, i.e., for areas A and B marked in Figure 4, respectively. (c) Positions of the DW [$x_{DW}(H_{ext}) - x_{DW}(H_{ref} = 21.9 \text{ kA/m})$] and [$y_{DW}(H_{ext}) - y_{DW}(H_{ref} = 21.9 \text{ kA/m})$] relative to its position for a reference field pulse of 21.9 kA/m as a function of field pulse amplitude H_{ext} . The scales in (a) and (b) are the same.

Kerr images - shift between reference and actual image*

without the shift



with +2 pixel shift
along y-axis



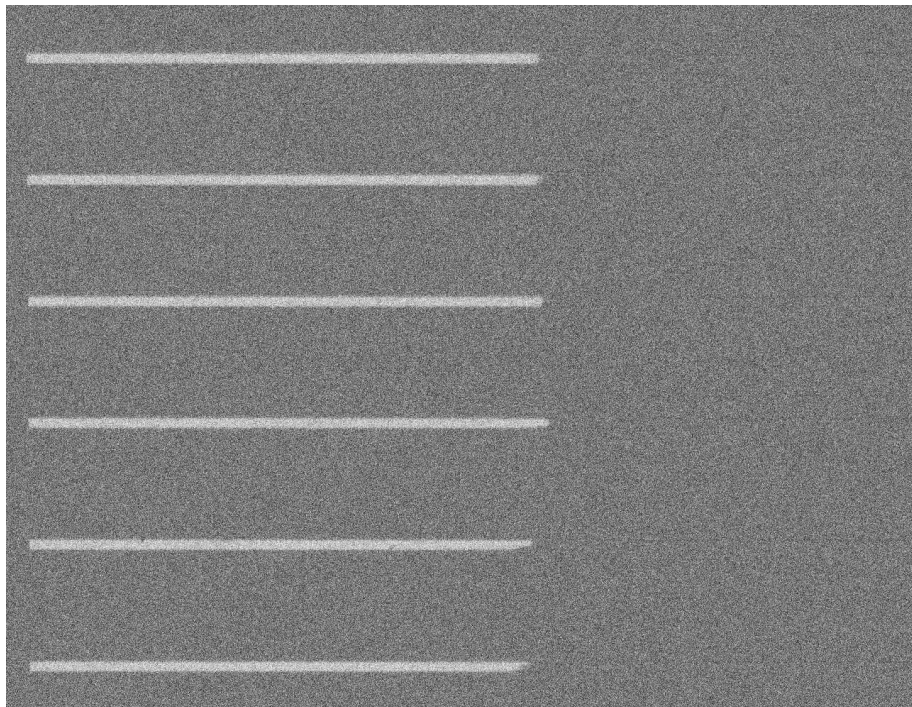
the edges become visible



*simulated images

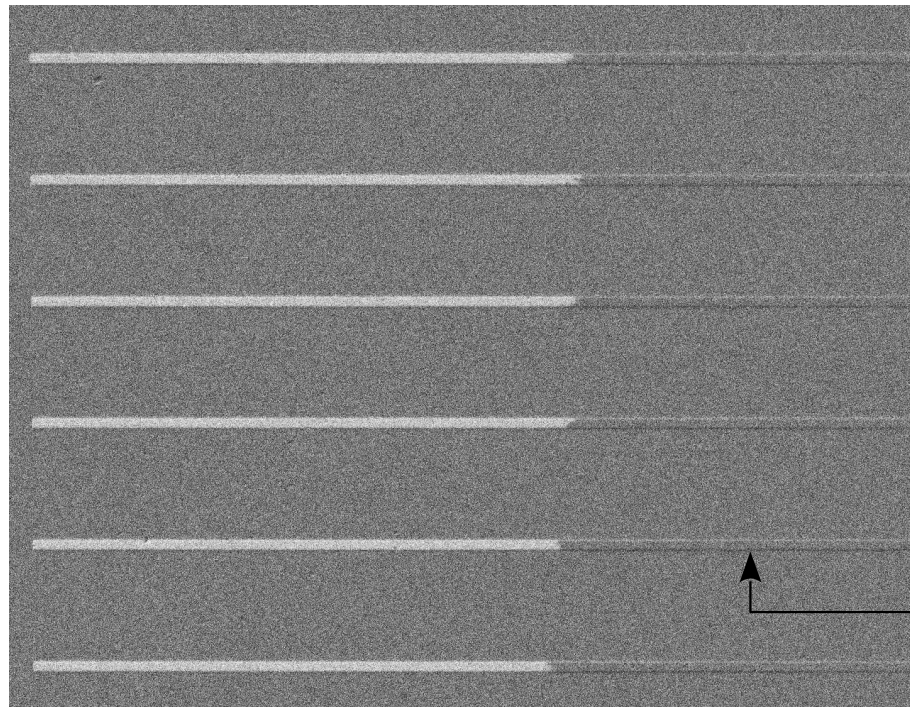
Kerr images - shift between reference and actual image

Kerr microscopy images of Si(100)/Ti(4nm)/Au(60nm)/[Co(0.8nm)/Au(1nm)]₂ film



with small shift

approx. 895×687 μm^2



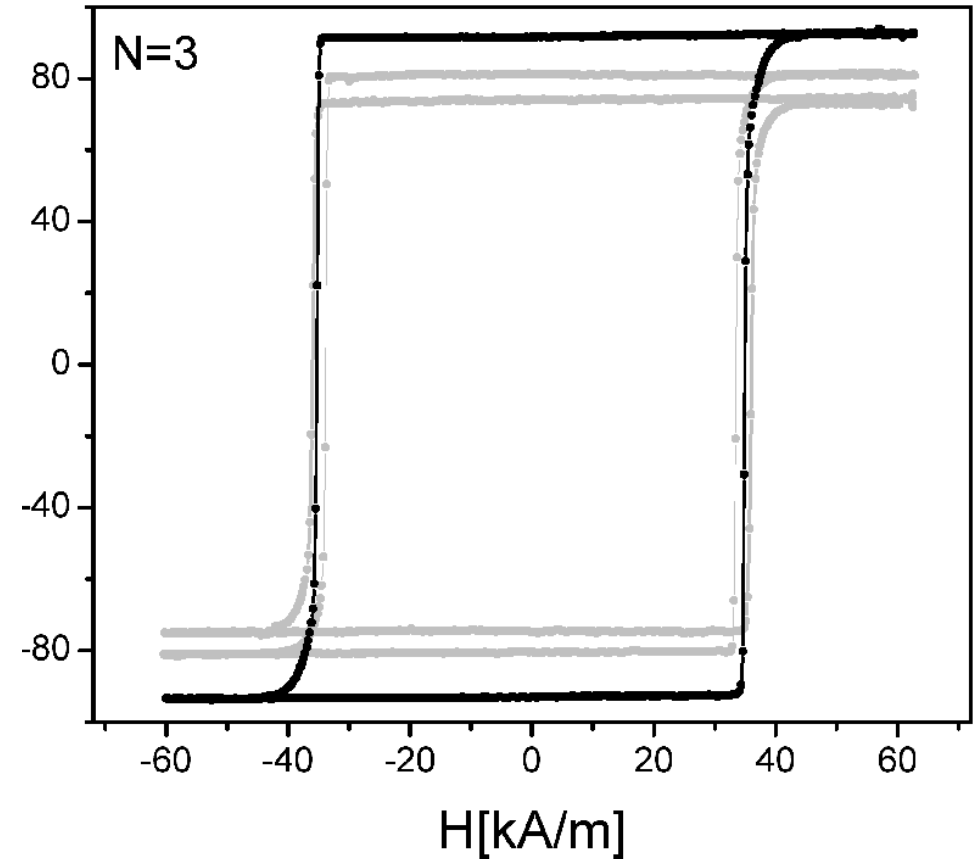
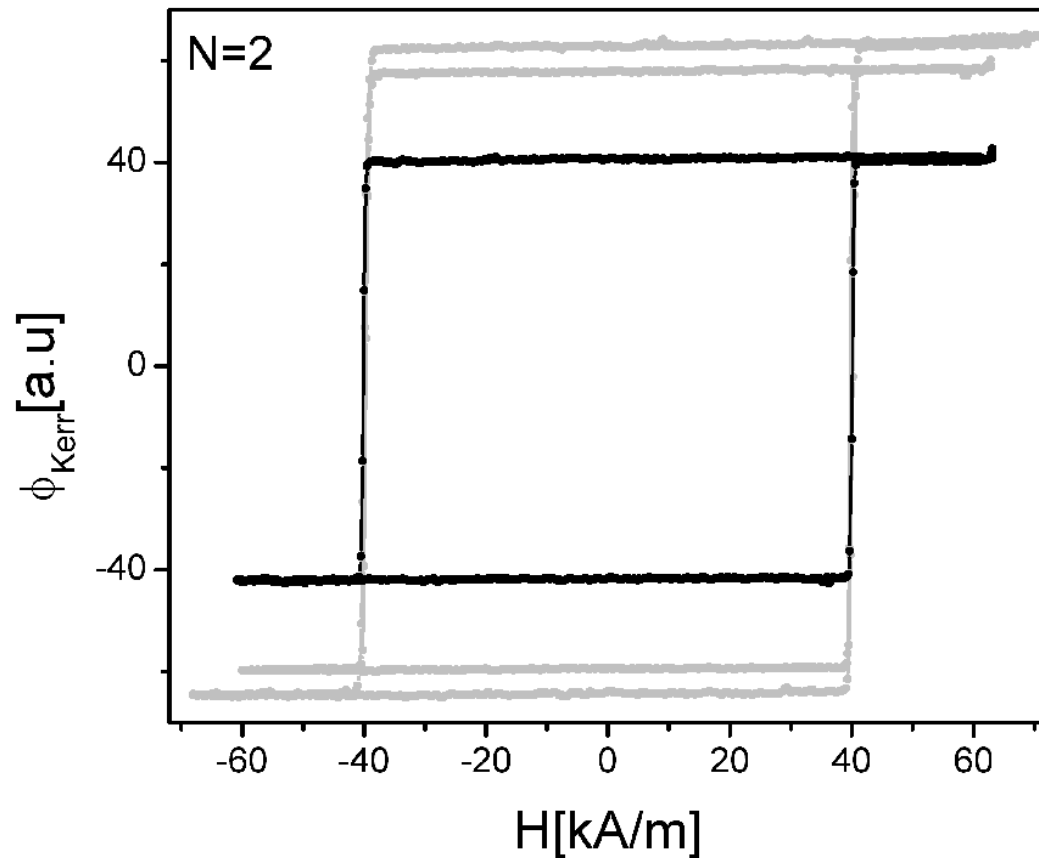
with a visible shift

no magnetic contrast here

Magnetic properties of extended sputtered $(\text{Co}/\text{Au})_N$ films

MOKE hysteresis loops of the $\text{Ti}(4\text{nm})/\text{Au}(60\text{nm})/[\text{Co}(0.8\text{nm})/\text{Au}(1\text{nm})]_N$ structures

Laser spot - 0.5mm diameter



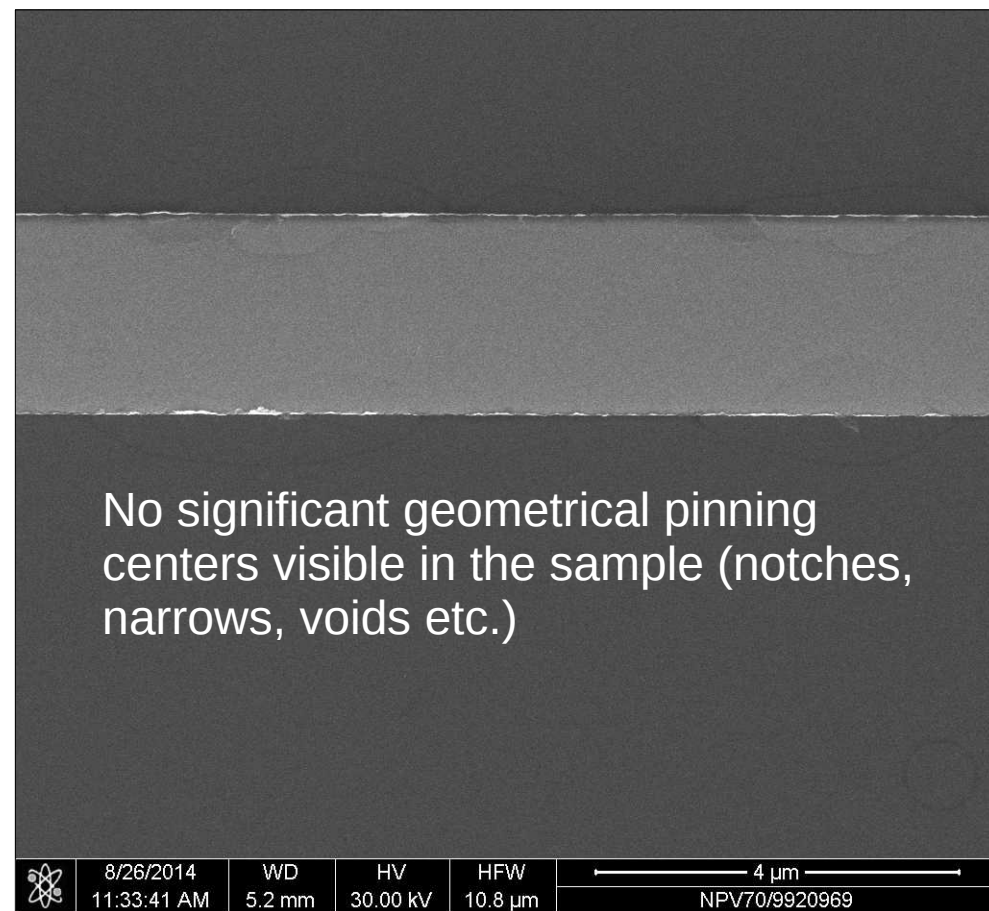
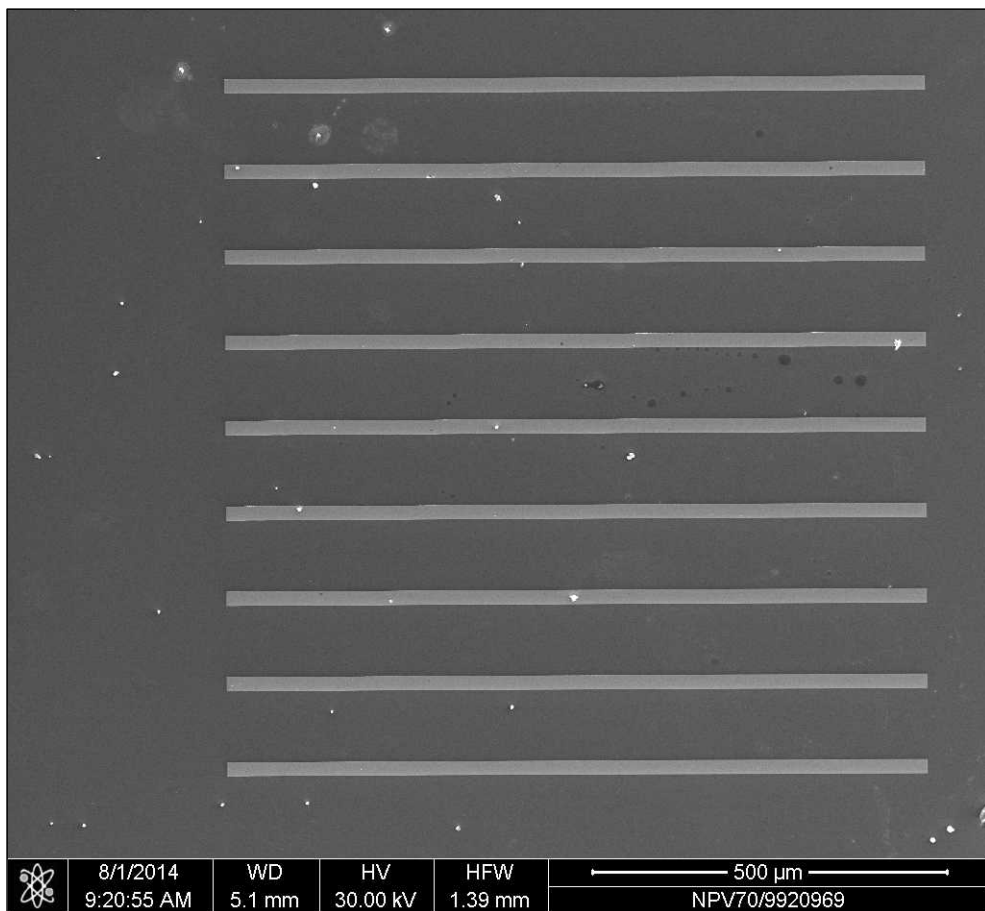
- $H_c(N=2) > H_c(N=3)$
- square hysteresis for $N=2$ - wall motion dominated reversal

Morphology of patterned sputtered $(\text{Co}/\text{Au})_N$ films

SEM images of the $\text{Ti}(4\text{nm})/\text{Au}(60\text{nm})/[\text{Co}(0.8\text{nm})/\text{Au}(1\text{nm})]_N$ structure

20 μm stripes on Si(100)

2 μm stripes



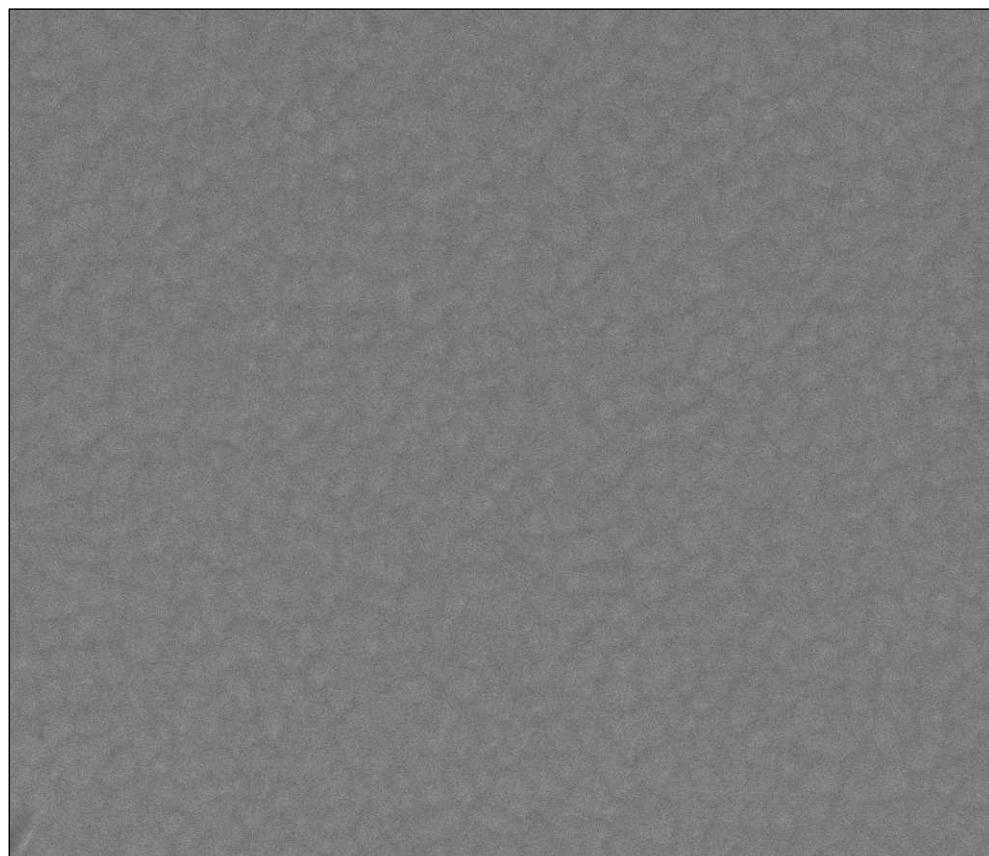
1 μm stripe



Structure of patterned sputtered $(\text{Co}/\text{Au})_N$ films

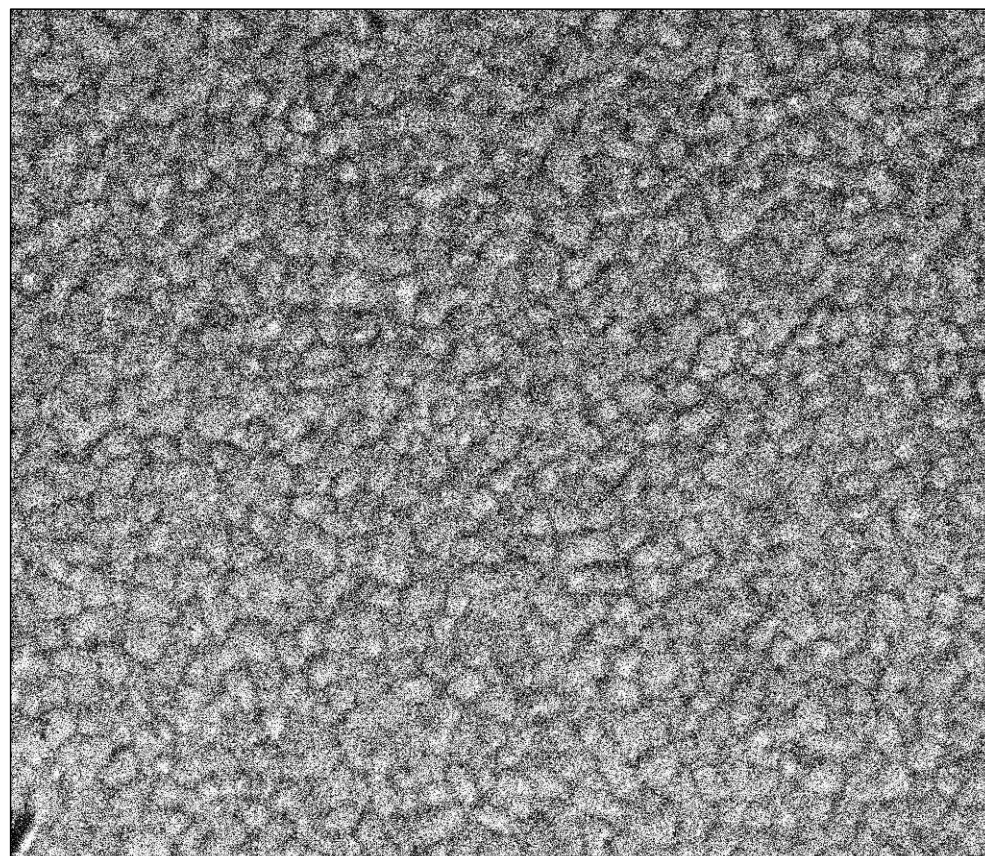
SEM images of the $\text{Ti}(4\text{nm})/\text{Au}(60\text{nm})/[\text{Co}(0.8\text{nm})/\text{Au}(1\text{nm})]_7$ structure

original image



	8/26/2014 11:35:01 AM	WD 5.2 mm	HV 30.00 kV	HFV 1.61 μm	500 nm	NPV70/9920969
--	--------------------------	--------------	----------------	---------------------------	--------	---------------

enhanced contrast



	8/26/2014 11:35:01 AM	WD 5.2 mm	HV 30.00 kV	HFV 1.61 μm	500 nm	NPV70/9920969
---	--------------------------	--------------	----------------	---------------------------	--------	---------------

columnar growth, grain diameters 50-100 nm

Ion bombardment for graded magnetic anisotropy

Procedure used in Z3/IFM PAN for large are samples [4]

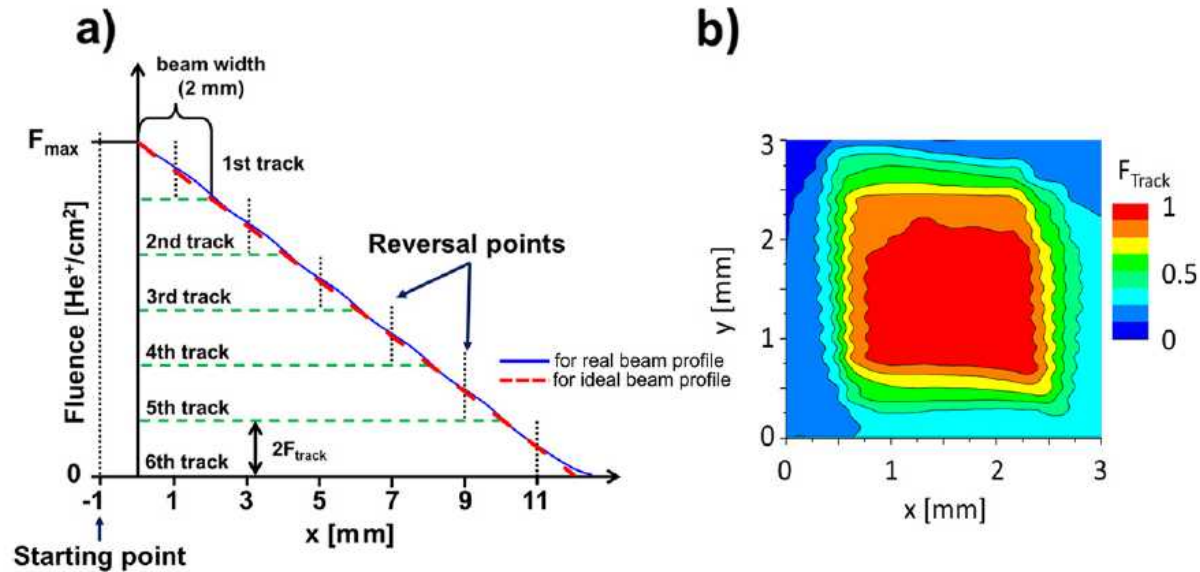


Figure 1 Fabrication of the monotonically varying ion fluence with defined ion beam profile. (a) Sketch of the ion bombardment procedure for constant fluence gradient along the x -direction. The cumulative fluence F versus x position after six tracks of an ion beam with the idealized rectangular intensity cross-section (dashed line) and the experimental intensity cross-section (solid line) of the beam profile shown in (b). The 'wavy' edges of the beam intensity at $x \approx 0.5$ and 2.5 are artifacts caused by measurement procedure (in which a Faraday cup with an opening of 0.1-mm diameter scans the beam along the x -direction).

Measurement procedure

- coercive field depends strongly on field sweep rate
- field sweep rate in our Kerr effect hysteresograph are about $1.4(\text{kA/m})/\text{s}$ (approx. 0.02 kOe/s)

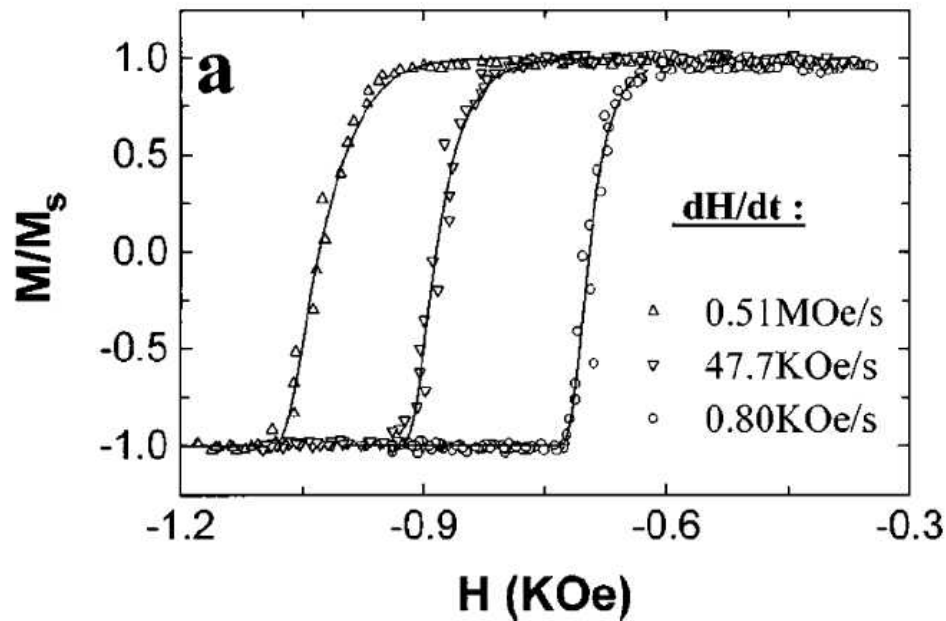


Fig. 4. Experimental hysteresis loops (open triangles) and simulated ones (full lines) measured on Au/Co/Au trilayers. A good agreement is found for low field sweep rates by using a SW barrier form with $\alpha = 1$. Reprinted figure with permission from B. Raquet, R. Mamy, J.C. Ousset, Phys. Rev. B 54 (1996) 4128–4136. Copyright 1996 by the American Physical Society.

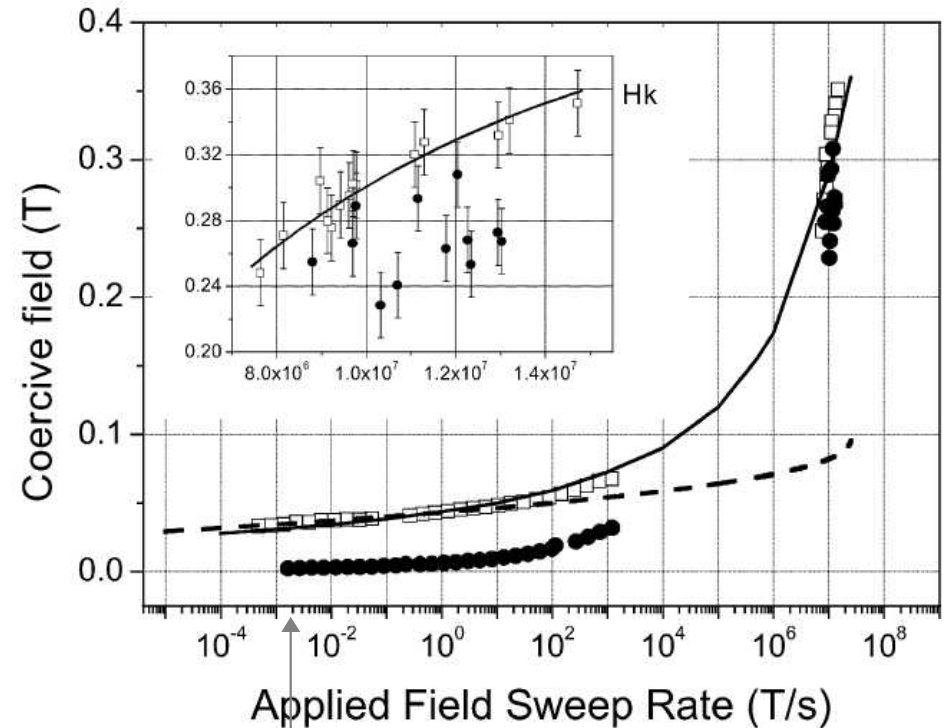
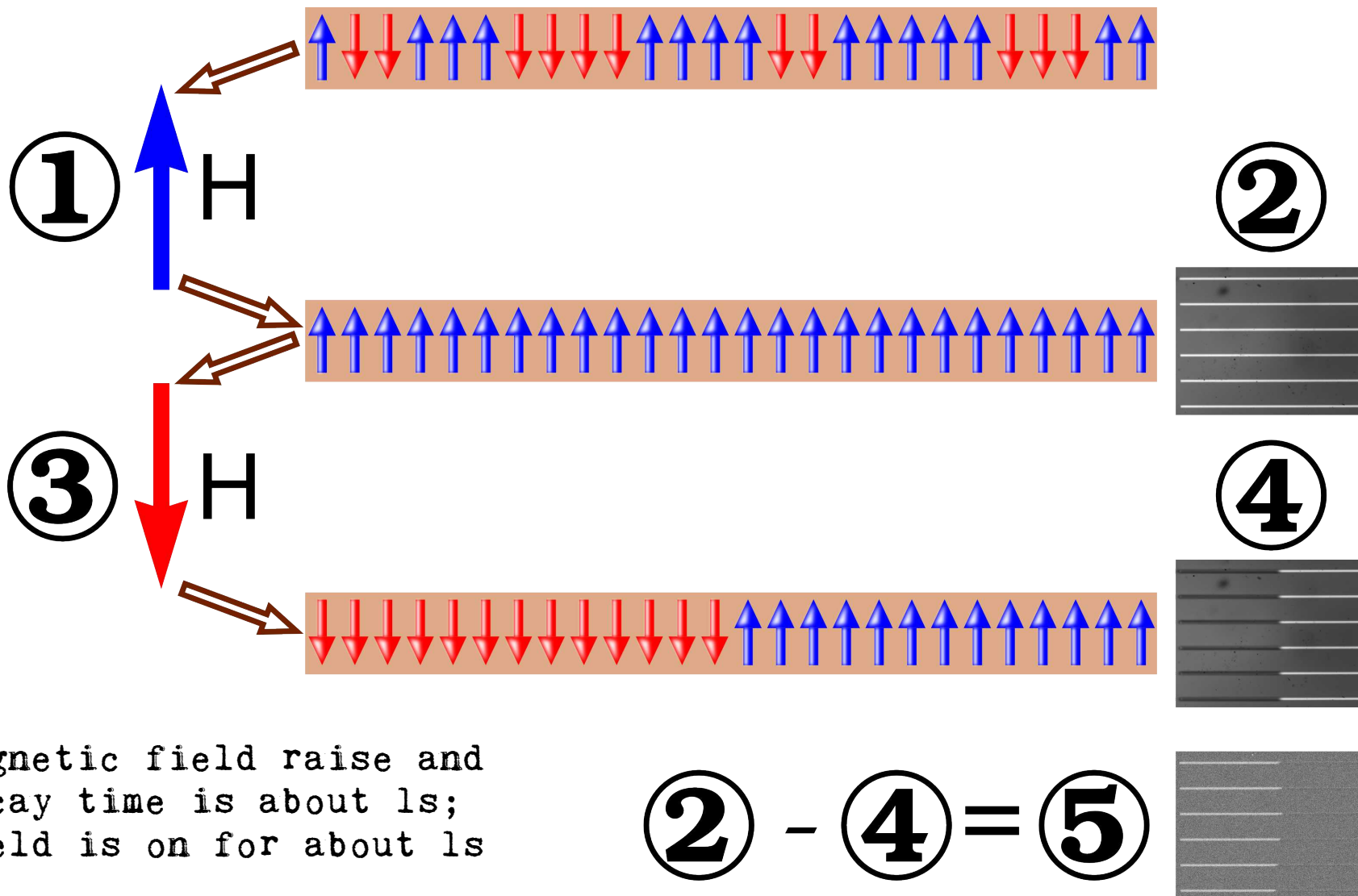


Fig. 5. Variation of the dynamical coercivity vs. the applied field sweep rate measured in continuous (dots) and patterned (squares) Co/Pt thin film multilayers. The continuous line represents the calculations of H_C using the droplet model; the dashed one is the calculated H_C deduced from the SW model. The inset shows a zoom for field sweep rates around 10^7 T/s (see Ref. [35]).

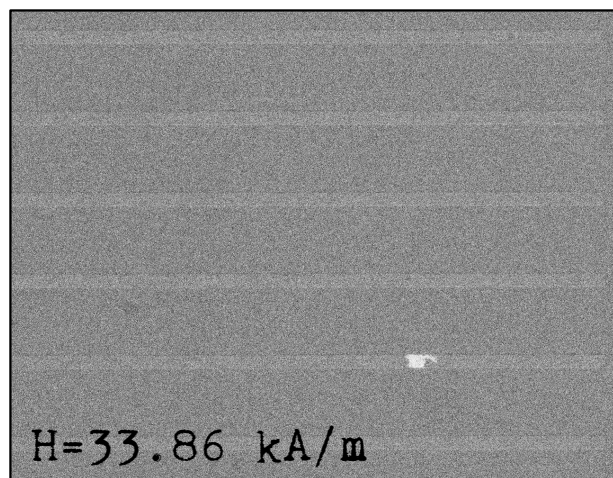
Measurement procedure

- We calculate the arithmetic difference between two images of the sample recorded for different magnetization configurations

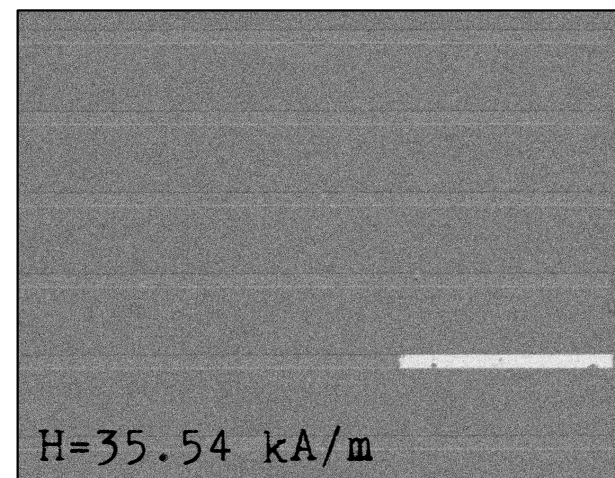
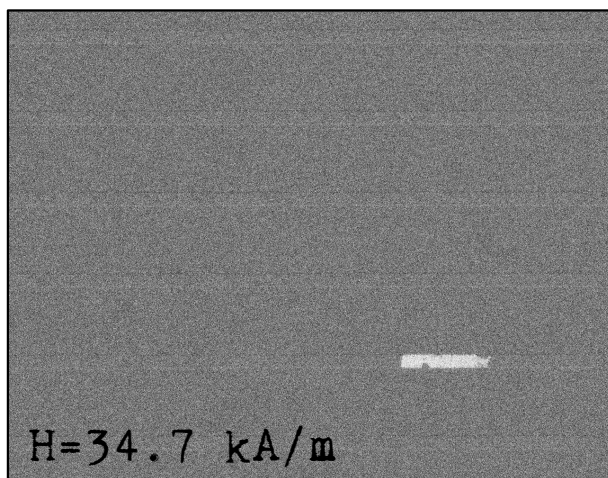


- Magnetic field raise and decay time is about 1s; field is on for about 1s

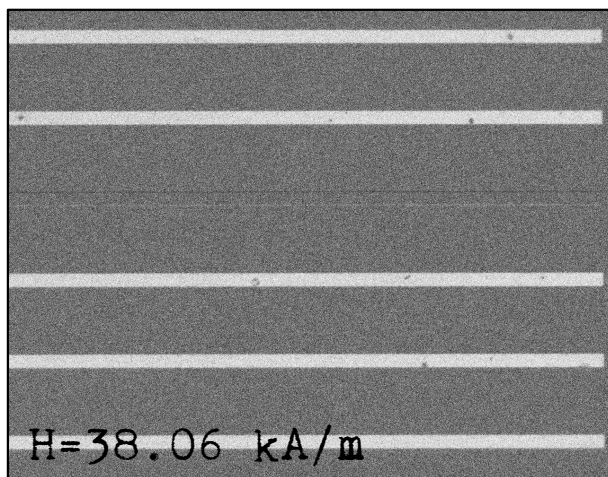
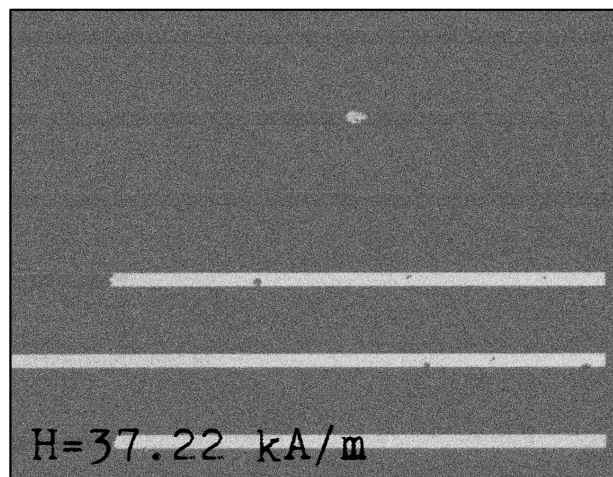
Magnetization reversal in as-deposited $(\text{Co}/\text{Au})_3$ stripes



approx. $895 \times 687 \mu\text{m}^2$



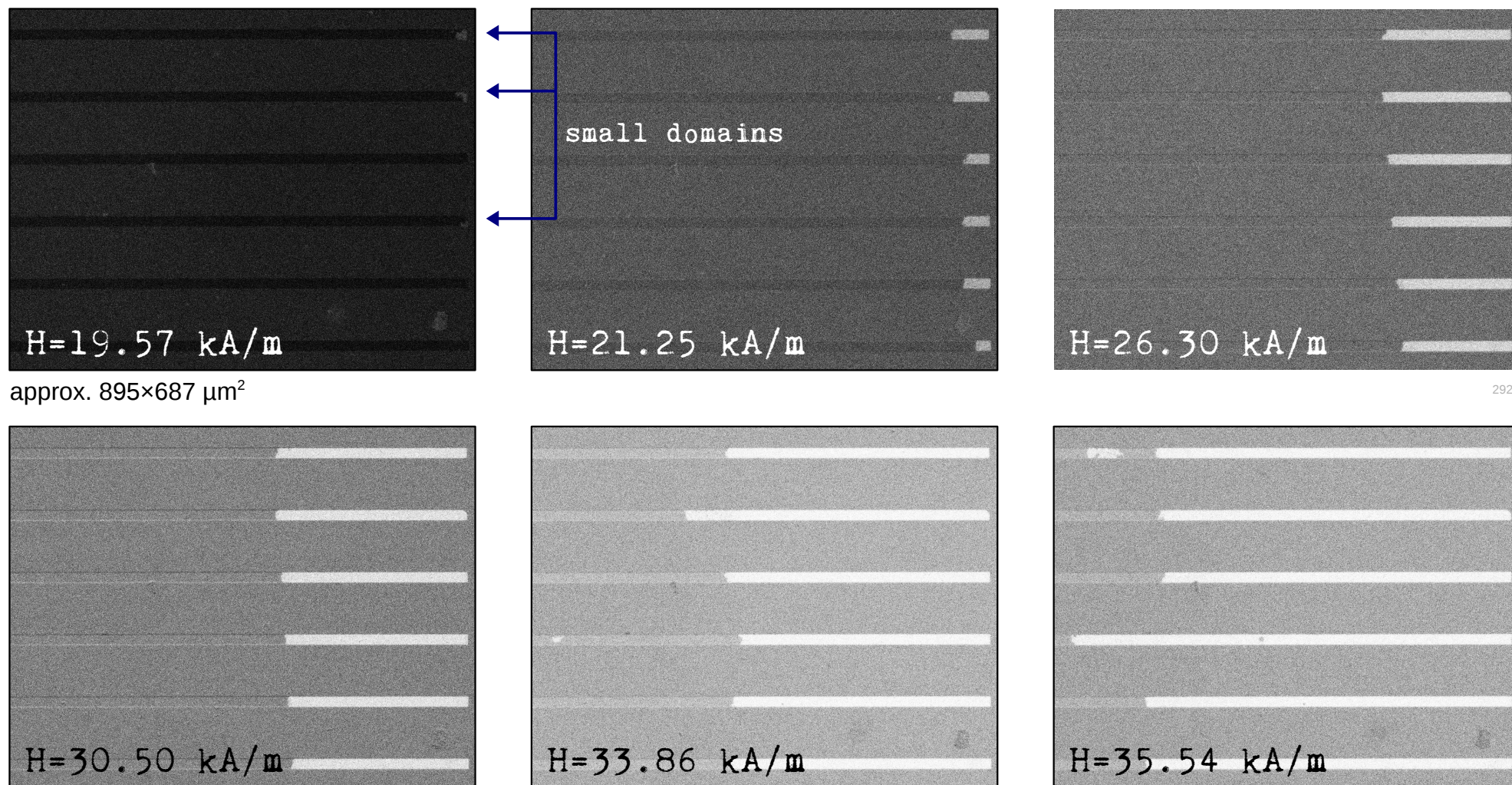
2929



no "active"
nucleation
center up to
38.06kA/m

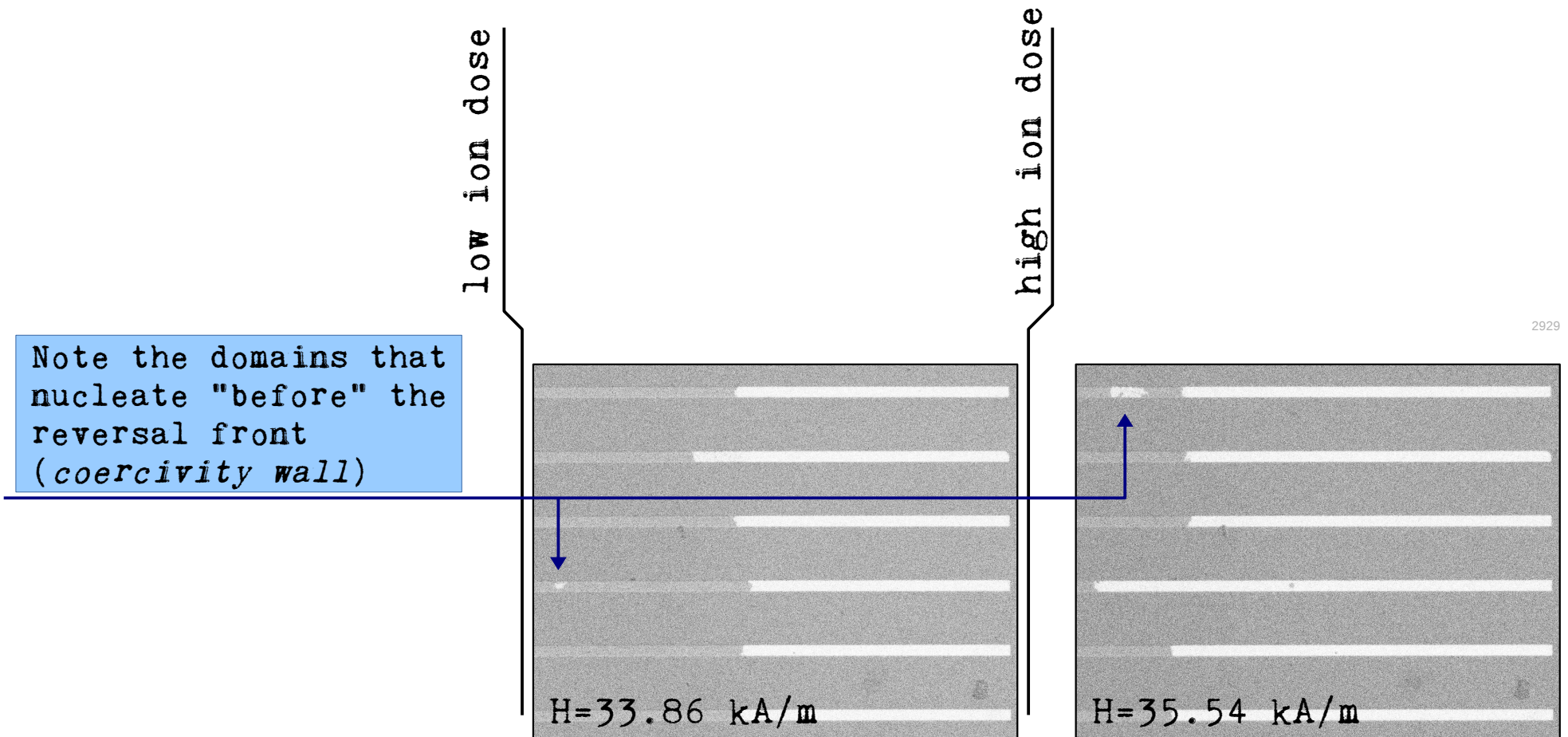
- In stripes that were not bombarded there is no visible preference for nucleation of domains in any specific area
- A possible preference for the direction of domain propagation may be a result of thickness gradient which is possible in thin films deposition
- Note the strong coupling between Co sublayers - single gray level of domain

Magnetization reversal in bombarded $(\text{Co}/\text{Au})_3$ stripes



- Reversed domains expand from right to left
- Note much wider field range (approx. 16 kA/m), as compared to the stripes that were not bombarded (approx. 4 kA/m, previous slide), in which the stripes are not in "single domain" state

Magnetization reversal in bombarded $(\text{Co}/\text{Au})_3$ stripes

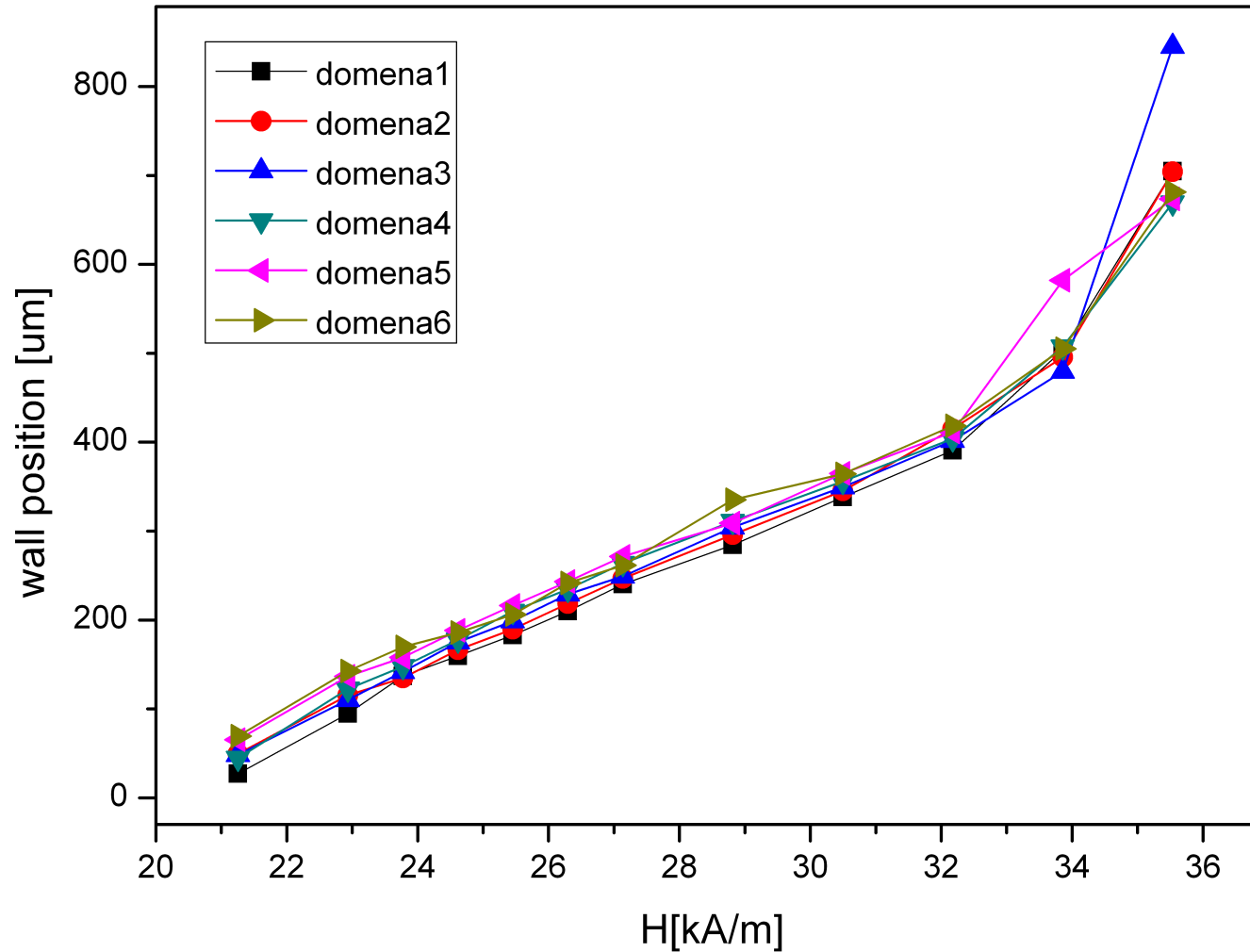


2929

- Reversed domains expand from right to left (**high dose** \rightarrow **low dose**)
- Note much wider field range (approx. 16 kA/m), as compared to the stripes that were not bombarded (approx. 4 kA/m, previous slide), in which the stripes are not in "single domain" state

Magnetization reversal in bombarded $(\text{Co}/\text{Au})_3$ stripes

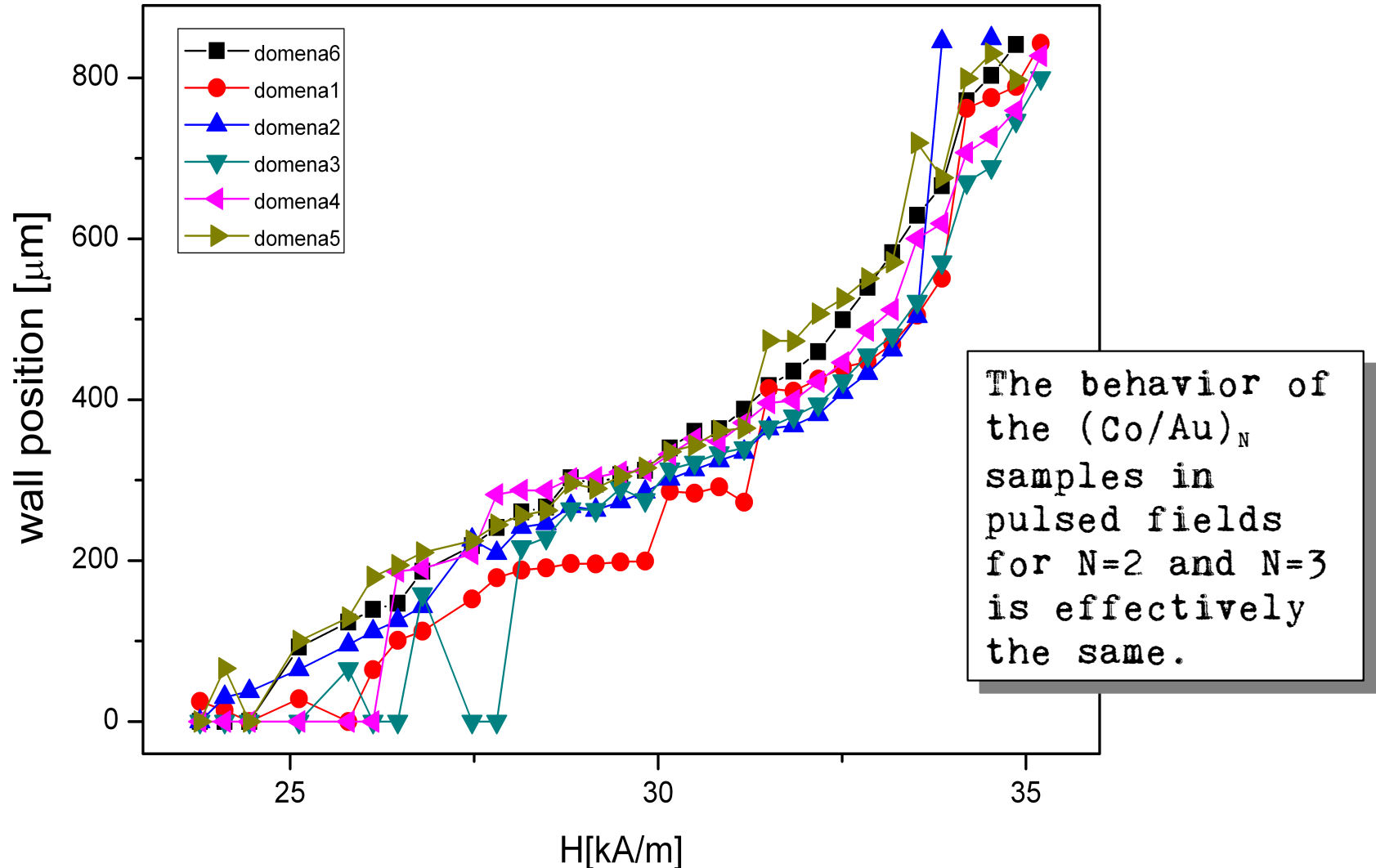
$N=3$



- In all stripes the domain wall position is approximately linear function of the magnetic field pulse strength H_p (for $H_p \ll H_c$)
- Global H_c of the extended reference sample is approx. 35 kA/m and H_s is over 40 kA/m.

Magnetization reversal in bombarded $(\text{Co}/\text{Au})_3$ stripes

$N=2$



- In all stripes the domain wall position is approximately linear function of the magnetic field pulse strength H_p (for $H_p \ll H_c$)
- Global H_c and H_s of the extended reference sample are approx. 40 kA/m (square loop)

Conclusions

- The He ion bombardment in patterned Co/Au MLs introduces analogous changes to those previously observed in extended films
- Controllable positioning of domain walls is possible
- The patterning seems to introduce nucleation centers into the film
- The nucleation sites seem not show up in the reversal of narrow stripes although the quality of imaging is low

References

- [1] I. Eichwald, S. Breitzkreutz, J. Kiermaier, G. Csaba, D. Schmitt-Landsiedel, M. Becherer, J. Appl. Phys. 115, 17E510 (2014)
- [2] A. Aharoni, Phys. Rev. B 45, 1030 (1992)
- [3] J. Vogel, J. Moritz, O. Fruchart, C. R. Physique 7, 977 (2006)
- [4] M. Matczak, B. Szymański, P. Kuświk, M. Urbaniak, F. Stobiecki, Z. Kurant, A. Maziewski, D. Lengemann, A. Ehresmann, Nanoscale Research Letters 9, 395 (2014)
- [5] J. Kimling, T. Gerhardt, A. Kobs, A. Vogel, S. Wintz, Mi-Y. Im, P. Fischer, H.P. Oepen, U. Merkt, G. Meier, J. Appl. Phys. 113, 163902 (2013)
- [6] THE INTERNATIONAL TECHNOLOGY ROADMAP FOR SEMICONDUCTORS: 2013
- [7] J.M.D. Coey, Magnetism and Magnetic Materials, Cambridge University Press 2009
- [8] P. Kuswik, A. Ehresmann, M. Tekielak, B. Szymanski, I. Sveklo, P. Mazalski, D. Engel, J. Kisielewski, D. Lengemann, M. Urbaniak, Ch. Schmidt, A. Maziewski, F. Stobiecki, Nanotechnology 22, 095302 (2011)
- [9] H. J. Williams, M. Goertz, J. Appl. Phys. 23, 316 (1952)